Microemulsion-Inspired Polysaccharide Nanoparticles for an Advanced Targeted Thrombolytic Treatment

Thibault de La Taille, Pierre Sarfati, Rachida Aid, Louise Fournier, Graciela Pavon-Djavid, Frédéric Chaubet, Cédric Chauvierre

Microemulsion-Inspired Polysaccharide Nanoparticles for an Advanced Targeted Thrombolytic Treatment

Thibault de La Taille [a], Pierre Sarfati [a], Rachida Aid [a, b], Louise Fournier [a], Graciela Pavon-Djavid [a], Frédéric Chaubet [a], Cédric Chauvierre [a,]*

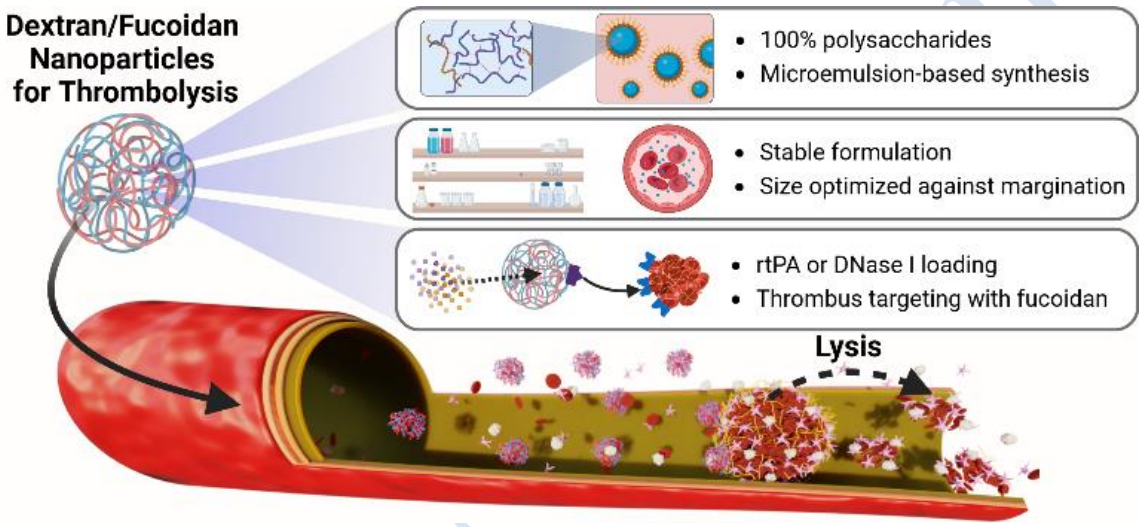

Keywords: Polysaccharides; Polymeric nanoparticles; Thrombotic diseases; Targeted thrombolysis; Drug delivery

[a] *UMR-S U1148 INSERM, Laboratory for Vascular Translational Science (LVTS), Université Paris Cité, Université Sorbonne Paris Nord, F-75018, Paris, France*

[b] *UMS 34, Fédération de Recherche en Imagerie Multi-modalité (FRIM), Université Paris Cité, F-75018, Paris, France*

** Corresponding author. E-mail address: cedric.chauvierre@inserm.fr (C. Chauvierre)*

Abstract

Among cardiovascular diseases, thrombotic diseases such as ischemic heart disease and acute ischemic strokes are the most lethal, responsible by themselves for a quarter of worldwide deaths. While surgical treatments exist, they may not be used in all situations and systemic thrombolytic drug injection, such as recombinant tissue plasminogen activators (rtPA), often remains necessary, despite serious limitations including short therapeutic window, severe side effects and failure to address the complex nature of thrombi. This prompted intense research into alternative thrombolytics or delivery methods, including nanomedicine. However, most nanoparticles face issues of stability, biocompatibility or synthesis robustness; among them, polymeric nanoparticles, though usually versatile and biocompatible, sometimes lack robustness and may involve toxic or complex synthesis. Here, we present polysaccharide hydrogel nanoparticles, designed with an improved microemulsion-based approach which allowed a critical size reduction from microparticles to 315 nm nanoparticles. They were decorated with fucoidan, a sulfated polysaccharide capable of high affinity binding to P-selectin, a thrombi biomarker. These nanoparticles exhibited a good stability, adequate size, biocompatibility and targeting capacity, and could be loaded with two different drugs, rtPA (fibrin degradation) or DNase I (degradation of neutrophil extracellular traps, or NETs), to exert thrombolysis. Notably, improved synergic thrombolysis was demonstrated on NET-containing thrombi, while *in vivo* thrombolysis shed light into improved thrombolysis of rtPA-loaded nanoparticles at 50% and 10% the recommended dose without secondary embolization. These safe, robust and easy-to-make nanoparticles could provide effective delivery strategies for thrombolytic treatments, while demonstrating the potential of polysaccharide nanoparticles as drug delivery agents.

Introduction

Cardiovascular diseases (CVDs) have been responsible for the most deaths worldwide in recent years, causing around 20 million deaths in 2021 alone.[1] Thrombotic diseases such as ischemic heart disease (IHD) and acute ischemic stroke (AIS) are the two top killers among them, and they remain respectively at the second and fourth place (behind COVID19 pandemic) in leading causes for disability-adjusted life years (DALYs) worldwide in 2021. There are multiple factors that can explain recent increasing trends in CVDs, including diabetes, high blood pressure, population aging, and health inequities among others. The burden of AIS and IHD is generally expected to continue increasing, making both prevention and improving therapeutic treatment critical. For ischemic diseases such as IHD and AIS, insufficient blood flow causes tissue infarction and usually results from thrombi (blood clots) occluding blood vessels in the heart (myocardial infarction, MI) or the brain (AIS).[2] While the exact composition of these thrombi can vary widely depending on the etiology and site of occlusion, they contain mostly fibrin, which is essential for the thrombus formation and mechanical strength, as well as various cell types including red blood cells (RBCs), immune cells or platelets.[2] However, other components were shown to be critical, such as Von Willebrand Factor (VWF) or neutrophil extracellular traps (NETs), which are DNA and protein networks released by neutrophils through a specific form of cell death known as NETosis.[3]

Several “clot busters” thrombolytic drugs exist. In the case of AIS, intravenous thrombolysis was introduced in 1995:[4] a recombinant tissue plasminogen activator (rtPA) enzyme, alteplase, is intravenously administered in order to activate plasminogen into plasmin, which will degrade fibrin in the thrombus. Despite its current place as a golden standard treatment, the drug half-life in circulation is less than 10 min, recanalization is low (around 20%),[5] and due to severe side effects (e.g., neurotoxicity, hemorrhagic transformations) and a short therapeutic window, only few patients are eligible: less than 10% AIS patients were treated with rtPA in the US in 2018.[6] In 2015, endovascular therapy (EVT) was introduced and demonstrated promising results, with a reported recanalization of more than 90% in certain patients;[7] however, it remains currently limited to large and medium vessel occlusions and therefore only 5% of all AIS patients in the US received EVT up to 2021, with few potentially eligible.[8] Furthermore, it has been

recently found that the complex composition and structure of thrombi might impair thrombolytic approaches,[3] with the extensive presence of NETs in AIS thrombi linked to rtPA resistance.[9] Notably, several groups have provided evidence that DNase I, which may degrade NETs, could improve the thrombolysis of arterial thrombi.[9–11]

Thus, multiple nanomedicine approaches have been reported to improve thrombotic disease treatment.[12,13] Indeed, the vectorization of certain drugs through nanoparticles (NPs) directly to the thrombus could increase drug circulation time, avoid systemic side effects and reduce the total drug amount to be delivered. Interestingly, the size and shape of NPs can affect their distribution inside the blood flow due to margination effects. In blood vessels, RBCs and similarly sized objects tend to circulate in the center, while smaller objects are pushed to the sides ("marginate"). However, below a size threshold in the hundreds of nanometers, NPs follow a plasma-like homogeneous flow distribution.[14–16] In contrast, below 100 nm NPs are generally most likely to extravasate or be internalized by endothelial cells, thus leaving the blood vessel.[17,18] Such behaviors could be used to either aim particles to the sides or to the center of the flow in blood vessels. Other innate properties of NPs can be useful, including increased surface-to-volume ratio, or emergence of certain physical properties (e.g., superparamagnetism and localized surface plasmon resonance).[13] Moreover, the targeting of such NPs to the thrombus is paramount to ensure a reduced drug use and a local increased activity. For blood clots, multiple biomarkers and adequate targeting moieties have been identified, including the RGD peptide for GPIIb-IIIa platelet receptors,[19] the CREKA peptide for fibrin,[20] or platelet membrane coating to mimic platelet recruitment to the clot.[21] Besides, the use of nanoplatforms also opens the way for multiple drug delivery, as explored by Xu *et al*., 2019, who co-delivered rtPA and a neuroprotection agent to the ischemic brain area,[22] theranostics with fluorescent nanoparticles with thrombolytic delivery from Niu *et al.*, 2020,[23] or simultaneous enzymatic and mechanical thrombolysis with the use of sonothrombolysis coupled with thrombolytic delivery through echogenic microbubbles.[24]

While multiple NP formulations exist, from inorganic particles to dendrimers or lipid-based, choosing one design is not straightforward. For instance inorganic NP are usually very stable, but their degradation and excretion can be problematic; dendrimers are multivalent tools useful for drug delivery, but have been burdened with toxicity issues;

lipid-based materials such as liposomes or lipid nanoparticles are very promising, but they involve complex mix of lipids, sometimes chemically modified, with robustness issues and high production costs.[13,25] On the other hand, polymeric particles are interesting because of their versatility and broad available materials, but can also face robustness and toxicity issues, due to the polymerizing or crosslinking agents, and eventual organic solvents involved in the synthesis.[13]

To propose a nanomedicine-based approach for thrombolysis, we designed targeted polysaccharide NPs that can be loaded with rtPA and DNase I. These particles are composed of polysaccharide hydrogels, and their synthesis through a microemulsion-inspired process yielded 315 nm NPs, while the one-pot synthesis was simple and involved only cost-effective, FDA-compliant reagents which satisfied green chemistry criteria. Notably, they were stable, were composed of biodegradable materials, and exhibited remarkable robustness throughout batch production. The targeting moiety was the fucoidan, a sulfated polysaccharide with nanomolar affinity for P-selectin, which is expressed on activated platelets and endothelium, and was demonstrated to be safe in humans with GMP formulation.[26–28] These NPs were fully characterized, including composition, stability, biocompatibility, targeting, the loading of two different drugs, rtPA and DNase I, and subsequent thrombolytic capacities, both *in vitro* and in a murine thrombosis model. Overall, these findings demonstrated the potential of polysaccharide NPs to deliver drugs to thrombi, validated the microemulsion-inspired framework for emulsion-based synthesis and opened perspectives for drug delivery through biocompatible polysaccharide NPs.

Results and Discussion

Nanoparticle synthesis

The synthesis consisted of a one-pot, two-step simple synthesis with robust production of uniformly sized NPs. It was inspired by previous protocols (referred to as “classical”) for formulating particles made up of polysaccharide hydrogels.[29,30] Notably, this protocol combines the chemical crosslinking of dextran with sodium trimetaphosphate (STMP) under alkaline conditions to form hydrogels, which was described elsewhere,[31] with the formation of stable water-in-oil (w/o) emulsion where water droplets serve as small reactors for hydrogel particle synthesis, as described in Fig.1.a; the crosslinking bonds

with STMP are phosphate diesters. Improvements were made by delaying the crosslinking reaction and, most importantly, by using the microemulsion (i.e., a thermodynamically stable emulsion) conceptualization of emulsions [32,33] to improve the w/o emulsion stability and diminish the water droplet size, thus reducing the resulting NP size. The Hydrophilic Lipophilic Difference (HLD) equation was used as presented by Abbott [32]:

$$(1) \qquad HLD = F(S) - k.EACN - \alpha.(T-25) + Cc$$

where F(S) represents a function of salinity S in the aqueous phase, EACN is the Effective Alkane Carbon Number determining the “oiliness” of oils, T is the temperature, Cc is the characteristic value of the surfactant, and k and α are fixed constants. When the HLD value is close to 0, the mixture obtained presents a balance between hydrophilic and lipophilic tendencies with extremely low interfacial tension, resulting in Type III Winsor emulsions. When HLD < 0, we obtain Winsor Type I oil-in-water (o/w) emulsions, and with HLD > 0, we obtain Winsor Type II w/o emulsions (Fig.1.b). In practice, these values can be determined from tables or determined experimentally, as shown in Fig.1.c, where a gradient in Cc values with two surfactants was prepared, thus obtaining a range of tubes displaying o/w emulsions (tubes 1 to 8, Fig.1.c), microemulsions (tubes 9 and 10, Fig.1.c) and w/o emulsions (tube 11, Fig.1.c). To form stable w/o emulsions, a strictly positive HLD value close to 0 was chosen. Through this framework, an adequate surfactant mix was determined to improve the emulsion step, with Cc = 2.39 and HLD = 0.80 (see HLD parameters in Sup.Fig.1). This synthesis yielded full dextran NPs, named Dex-NPs, and 5 wt.% fucoidan-incorporating dextran NPs, named Fuco-NPs, to serve as targeting NPs. The Z-average hydrodynamic diameter was respectively 313.7±14.4 nm and 316.5±15.3 nm, with low dispersity (polydispersity index, or PDI, considered as monodisperse below 0.2) as measured by Dynamic Light Scattering (DLS), without significant differences between both formulations (Sup.Fig.2). When comparing the former “classical” formulation to the microemulsion-based optimized formulation, the synthesis yielded batches in a robust manner with narrow Z-average size distribution which retained the same dispersity throughout batches (Fig.1.d-e, Sup.Fig.2), with an overall size reduction from around 850 to 315 nm. Sphericity was also confirmed by TEM (Sup.Fig.3). Furthermore, a major challenge with NPs remains their stability in various

colloidal suspensions, with stabilizing agents often used. As shown in Fig.1.f, with the “classical” submicronic particles, size increase through aggregation and sedimentation is seen when resuspended in saline without addition of the surfactant Tween 20; in contrast, with the optimized protocol, the Fuco-NPs do not show any significant differences in size in ultrapure water, saline, or saline with a stabilizer. These results validate the use of a microemulsion model to improve the formulation: a significant size reduction of NPs was obtained while using a similar protocol similar to the “classical” one which previously yielded micron-sized particles.[29,30] It also guaranteed a robust process with low inter-batch variability. Interestingly, the protocol improvement also resulted in increased stability of NPs without using stabilizing agents and without significant size variation even when the solvent ionic strength increases, in contrast to the previous “classical” particles.

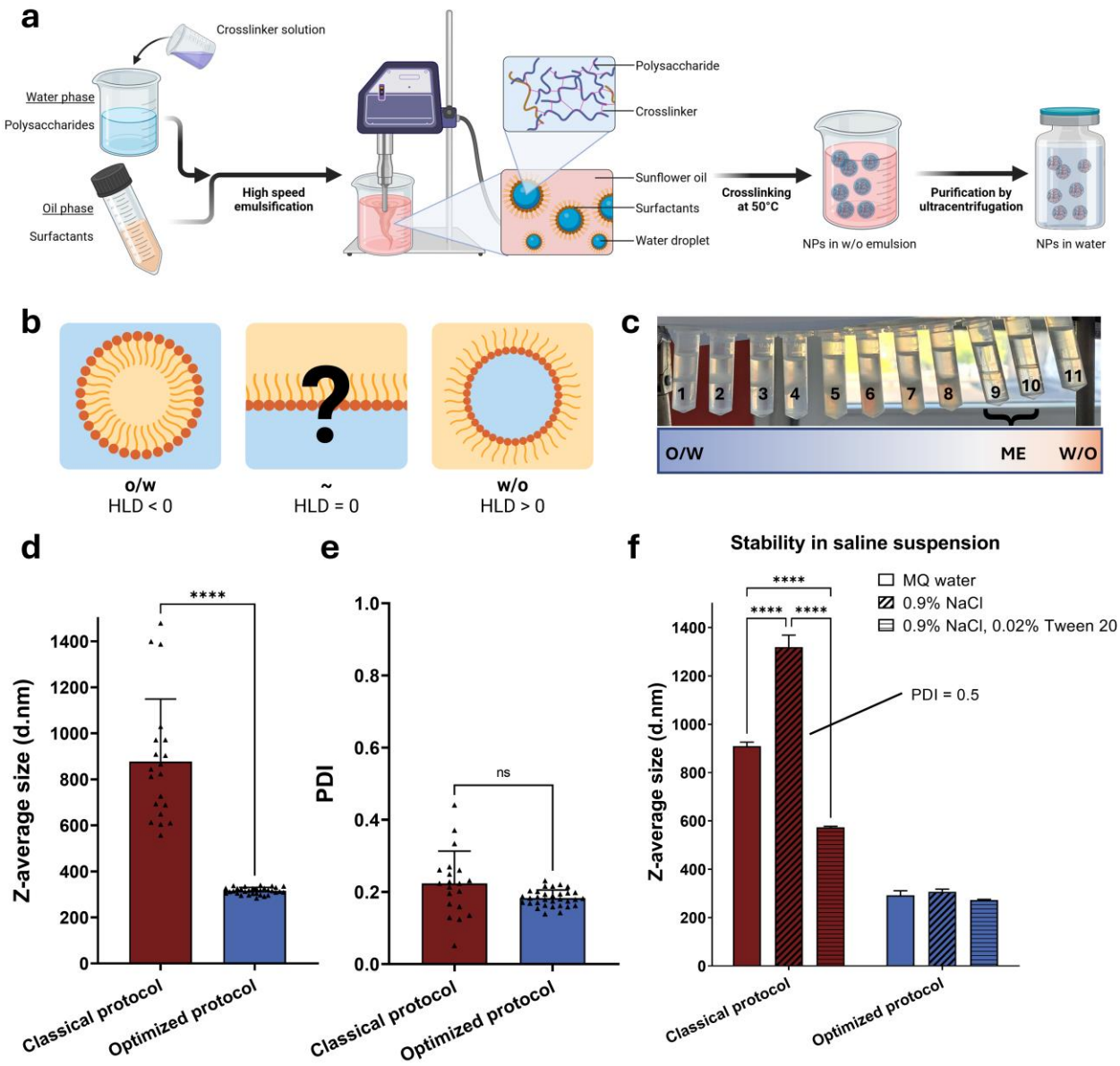

Figure 1. *Synthesis of Dex-NPs and Fuco-NPs. (a) Description of the one-pot synthesis process. A water phase containing the polysaccharides, NaCl and NaOH, is mixed with the STMP crosslinker, and then added dropwise in the oil phase constituted of sunflower oil and surfactants. The emulsification is performed with a high-speed homogenizer at 30 000 rpm on ice for 2.5 min followed by transfer in a 50 °C oven for crosslinking. The resulting NPs are purified and isolated by multiple rounds of ultracentrifugation. (b) Thermodynamic emulsion behavior of water and oil depending on Hydrophilic Lipophilic Difference (HLD) values (right). (c) Representative microemulsion scan based on sunflower oil, water, and a mix of surfactants displaying a microemulsion (ME) in tubes 9 and 10. The surfactant mix is performed such that the HLD is increasing from left to right. (d-e) Comparison of particle size (d) and dispersity (e) between the*

classical (n = 21) and final (n = 32) protocols. (f) Size comparison of fucoidan containing particles between classical particles and Fuco-NPs in water, saline or saline with 0.02% Tween 20 as surfactant. When not indicated, the PDI was below 0.2. A two-way ANOVA was performed, with Tukey's multiple comparison test to compare only the suspension medium effects (n = 3).

Nanoparticle characterization

The size and PDI of Dex-NPs and Fuco-NPs are recapitulated in Fig.2.a and were obtained in similar yields. The surface charge of NPs was measured as it often plays a major role in colloidal stability. Across a broad pH range, the Zeta potential measured by Electrophoretic Light Scattering (ELS) was below -20 mV for Dex-NPs and below -25 mV for Fuco-NPs (Sup.Fig.4), with specifically the Zeta potential at neutral pH of -25.9 ± 1.2 mV for Dex-NPs and -32.2 ± 1.8 mV for Fuco-NPs. The phosphorus and sulfur content were measured by TXRF, which respectively validated the incorporation of phosphorus through the phosphate diester crosslinking bonds, and incorporation of sulfate-containing fucoidan in Fuco-NPs. Similar Fourier transform infrared (FTIR) spectra (Sup.Fig.5) also demonstrated that Dex-NPs and Fuco-NPs were both fully constituted of polysaccharides (fucoidan being mostly indistinguishable from dextran by FTIR). Being made of dextran, a neutral polysaccharide, the low Zeta potential of NPs also clearly indicated the incorporation of negatively charged components: the phosphate diester crosslinking bonds, and fucoidan; such negative surface charges are generally considered low enough to impart electrostatic colloidal stability. This was verified by the storage stability of Fuco-NPs evaluated by size measurements over a year at 4 °C (Fig.2.b). Besides, freeze-drying of Fuco-NPs in 1% sucrose was possible without loss in size or dispersity as verified in Sup.Fig.6. This long-term cold storage and freeze-drying capacity are especially interesting for logistic and pharmaceutical purposes. Furthermore, the size of circulating objects can be crucial for their behavior in the blood, due to the margination effects previously mentioned. To verify whether the size reduction from 850 to 315 nm could affect the particle distribution profile inside blood vessels, they were flown in blood at a venous flow rate in microfluidic channels. As shown in Fig.2.c, while 850 nm "classical" particles demonstrated a typical margination to the sides of the channel, the optimized Fuco-NPs presented a homogeneous profile across the microfluidic vessel cross-section. This can help warrant access to the thrombus wherever its location in a blood vessel, and keep NPs in the circulation.[15,34] Thus, these NPs fall in a desirable size

range of 150-400 nm in order to avoid extravasation [18] while maintaining them homogeneously distributed in blood flow.[15,34] In addition, the Fuco-NPs' in flow distribution after 30 min incubation in whole human blood was similar, suggesting the lack of aggregation or significant size increase, as shown in Sup.Fig.7. To further validate the use of these NPs, their biocompatibility was assessed. As they are meant to interact in the circulation, cytotoxicity was evaluated by measuring the metabolic activity by resazurin reduction after 24 h incubation of HUVEC endothelial cells in contact with the Fuco-NPs, as shown in Fig.2.d, where all concentrations assayed displayed a viability above the 70% threshold (decided as per ISO 10993-5 [35]), with notably the highest assayed concentration, 1000 µg/mL Fuco-NPs, displaying a 92.8 ± 5.7% viability. PBS was used as a control to compare effects of different medium dilutions. Moreover, HUVEC cell morphology was verified after incubation of 100, 400, 800 (not shown) and 1000 µg/mL Fuco-NPs for 24h (Fig.2.e): the cells retained the cobblestone aspect and preservation of the actin cytoskeleton when comparing PBS exposure to Fuco-NPs. Finally, since the Fuco-NPs are meant to be circulating, the absence of hemolytic properties was essential. Both Dex-NPs and Fuco-NPs showed no hemolytic properties when incubated with human RBCs (10% being the threshold for nonhemolytic, and >25% for hemolytic risk [36]) as shown in Sup.Fig.8. Besides, the biodegradability of Fuco-NPs by a (1 → 6)-α-D-glucosidase (such as dextranase), the activity of which is present in human tissues,[48–50] was measured. As shown in Sup.Fig.9, dextranase could degrade 100% of Fuco-NPs in 1 h at RT. This suggests that *in vivo* biodegradation of Fuco-NPs is possible.

a

	Z-average size (d.nm)	PDI	Concentration post synthesis (g/L)	Zêta potential at pH = 7 (mV)	Fucoidan content (wt.%)	Phosphorus content (wt.%)
Dex-NPs	313.7 ± 14.4	0.18 ± 0.02	1.4 ± 1.0	- 25.9 ± 1.2	-	1.0 ± 0.3
Fuco-NPs	316.5 ± 15.3	0.18 ± 0.03	1.8 ± 0.8	- 32.2 ± 1.8	4.4 ± 2.0	1.3 ± 0.4

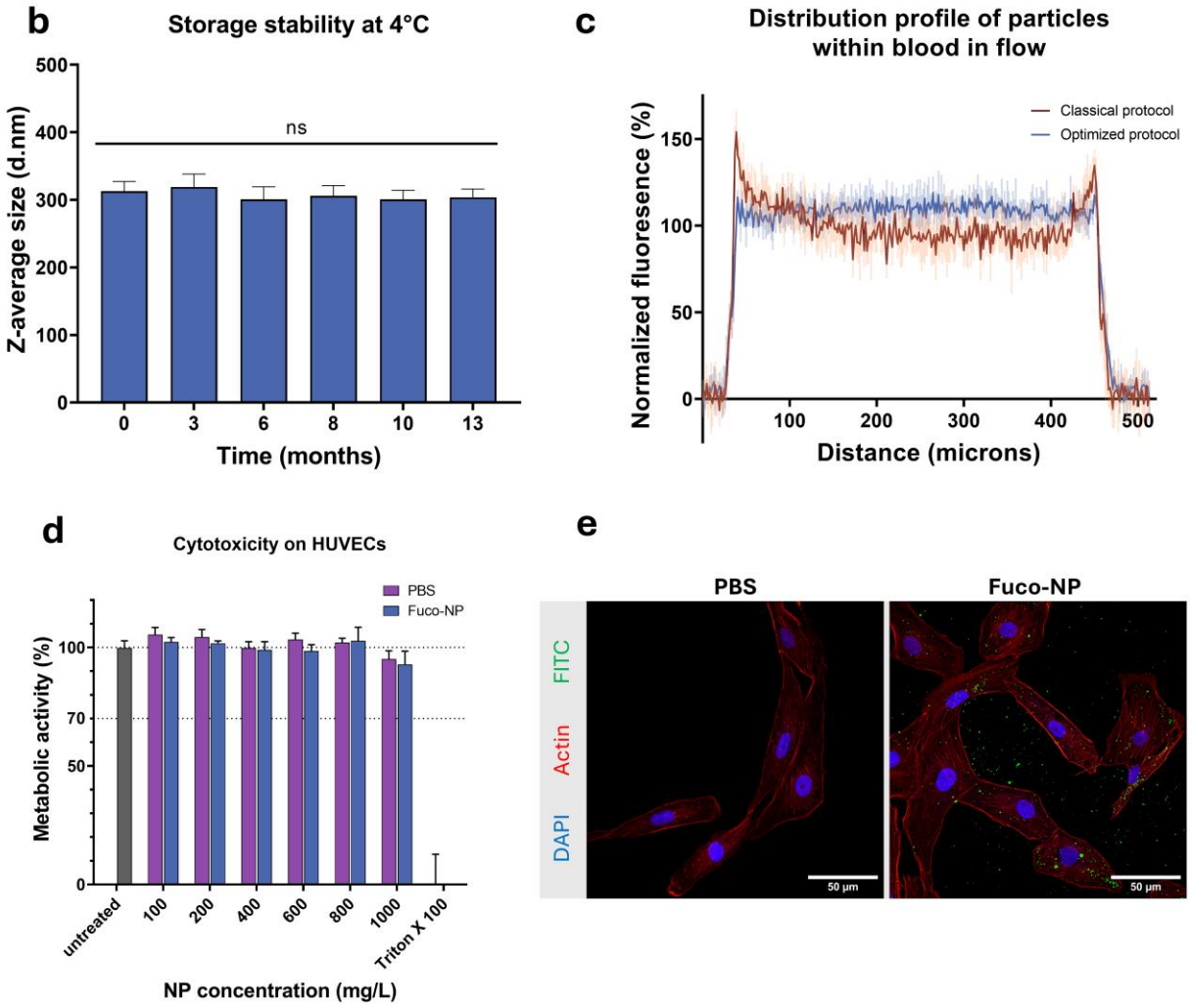

Figure 2. *Characterization of NPs. (a) Major physico-chemical characteristics of Dex-NPs and Fuco-NPs. The fucoidan and phosphate contents presented were obtained by TXRF. (b) Z-average size comparison measured by DLS for batches with different storage times at 4 °C. One-way ANOVA with Dunnett's multiple comparison test to compare every column to t = 0 was performed (n ≥ 3). (c) In flow behavior comparison of fucoidan containing 850 nm particles, obtained with the classical protocol, with 315 nm Fuco-NPs (optimized protocol). The blood containing 1 mg/mL TRITC-tagged particles is flowed at a venous flow rate in a microfluidic channel, and the fluorescence signal across a cross-section of the channel is measured. The X-axis corresponds to the cross-section distance (n = 5). (d) Cytotoxicity test performed by*

measuring human umbilical vein endothelial cells (HUVECs) viability through the metabolic activity by resazurin after 24 h incubation with Fuco-NPs or PBS (similar medium dilution as a control). Triton X-100 1% for 15 min served as a positive control and was significantly different from all others (not shown for clarity); the analysis was a 2-way ANOVA with Tukey's multiple comparison test to compare only the differences between PBS and Fuco-NPs (n = 4). (e) HUVEC morphology after 24 h incubation with 1 mg/mL FITC-labeled Fuco-NPs visualized with the nuclei (DAPI) and actin (rhodamine phalloidin) (scale bar = 50 µm).

Drug loading

Once the NPs were fully characterized, the loading of various drugs by simple adsorption, including rtPA and DNase I, was investigated. Notably, the loading capacity (LC (%) = [drug loaded]/[NP]) was measured by BCA (total protein quantification) across various rtPA and Fuco-NP concentrations, as displayed in Fig.3.a. For a fixed 2.5 mg/mL Fuco-NP concentration, co-incubation with 0.25 mg/mL rtPA yielded the highest LC. This loading condition was kept in all further experiments, and the resulting loaded NPs were designed as Fuco-NP-rtPA, with a LC of 6.7 ± 0.6% (Fig.3.c). Interestingly, it was observed that, in similar loading conditions, rtPA loading was significantly increased in Fuco-NPs, due to a previously undescribed affinity of rtPA to fucoidan,[37] compared to Dex-NPs (Fig.3.c). Moreover, the release of rtPA was investigated in PBS at 37 °C, at a dilution corresponding to the injection of a 1 mg/kg rtPA dose in mice (10 times lower than the effective dose usually used [38]) or equivalent to 0.9 mg/kg dose of rtPA in humans, the current clinical recommendation for AIS treatment.[4] As shown in Fig.3.d, a release curve illustrative of a burst release in the first 15 min and reaching a complete release after 60 min was obtained. The amidolytic activity of rtPA after loading was validated with a fluorescent substrate assay (PefaFluor) as shown in Sup.Fig.10 and was retained after freeze-drying and resuspension without destabilizing the Fuco-NPs, with only a minor size decrease (Sup.Fig.10 and Sup.Fig.12). However, under the same loading conditions, barely any DNase I was loaded in Fuco-NPs. The isoelectric point of rtPA is around 7.5, while the isoelectric point of Pulmozyme (the DNase I used) is reported at 4.6, meaning that at neutral pH, rtPA is either neutral or slightly positively charged, while DNase I is negatively charged, which could prevent loading onto Fuco-NPs by electrostatic repulsion. As the latter remained negative across a broad pH range (Sup.Fig.4), loading at different pH values was tested (see Sup.Fig.11.a), demonstrating a successful

adsorption of DNase I at pH = 3. Based on this acidic condition, various DNase I and Fuco-NP conditions were tested, with notably the incubation of 0.5 mg/mL DNase I with 2.5 mg/mL Fuco-NP yielding the highest LC (Fig.3.b). This condition was used in all following experiments and labeled Fuco-NP-DNase: the LC of DNase I was 16.9±0.4%. This LC remained similar for both Dex-NP-DNase and Fuco-NP-DNase (Fig.3.e), with a release profile similar to that of rtPA (Fig.3.f). However, such acidic conditions could denature DNase I, and therefore a fluorescent DNA substrate kit was used to measure the DNase I activity after loading onto Fuco-NPs and in acidic conditions (Sup.Fig.11.b). This demonstrated that while acidic exposure significantly reduced DNase I activity by 12-fold, activity was partially preserved in Fuco-NP-DNase with only a 2.5-fold reduction in activity. This amounted to an effective LC (measured as [active drug]/{NP]) of 8.3±2.2%. Fuco-NP-DNase freeze-drying further reduced the active drug content (Sup.Fig.11.b), to a corresponding effective LC of 4.7±2.5%, but Fuco-NP-DNase remained stable, with only a minor size decrease (Sup.Fig.12). Co-loading rtPA and DNase I in the same NPs was tested with no success, as rtPA loading always prevailed on DNase I (Sup.Fig.13), and thus Fuco-NP-rtPA and Fuco-NP-DNase were prepared separately and assembled immediately before each further experiment. Even though the rtPA and DNase I enzymatic activity was assessed with fluorescent substrate assays, it did not necessarily guarantee that they can still fulfill their fibrinolytic or NETolytic activity. Thus, two respective models were designed. On the one hand for rtPA, a fibrin agar plate assay (FAPA) was used.[39] The degradation ring's rate of expansion was measured (Sup.Fig.14) and with a standard range of free rtPA, the active amount of rtPA in a sample could be determined. As shown in Fig.3.g during loading experiments, the amount of active drug loaded in Fuco-NP was measured at 201 ± 23 µg/mL, slightly above the rtPA amount determined by BCA, indicating that the loaded rtPA retained its fibrinolytic potential. On the other hand for DNase I, a NETolysis assay was designed based on previous works.[40] Neutrophils were isolated from human blood and then activated with PMA. SytoxGreen and DAPI DNA dyes were used after various treatments, owing to SytoxGreen lack of intracellular penetration compared to DAPI, to distinguish extracellular DNA (NETs) from nuclear DNA. After 4 h activation, the NETs were incubated with the Fuco-NP-DNase samples or with free DNase I. As shown in Fig.3.h top panels, NETs could be clearly seen after PMA activation. NETolysis could be observed in a DNase I

concentration-dependent manner, and at equal amounts of DNase I of 0.5 µg/mL, both free DNase I and Fuco-NP-DNase produced similar degradation of the NETs (Fig.3h bottom panels). This validated the NETolysis activity of DNase I on human NETs, but it also confirmed the retained activity of DNase I after loading in Fuco-NPs.

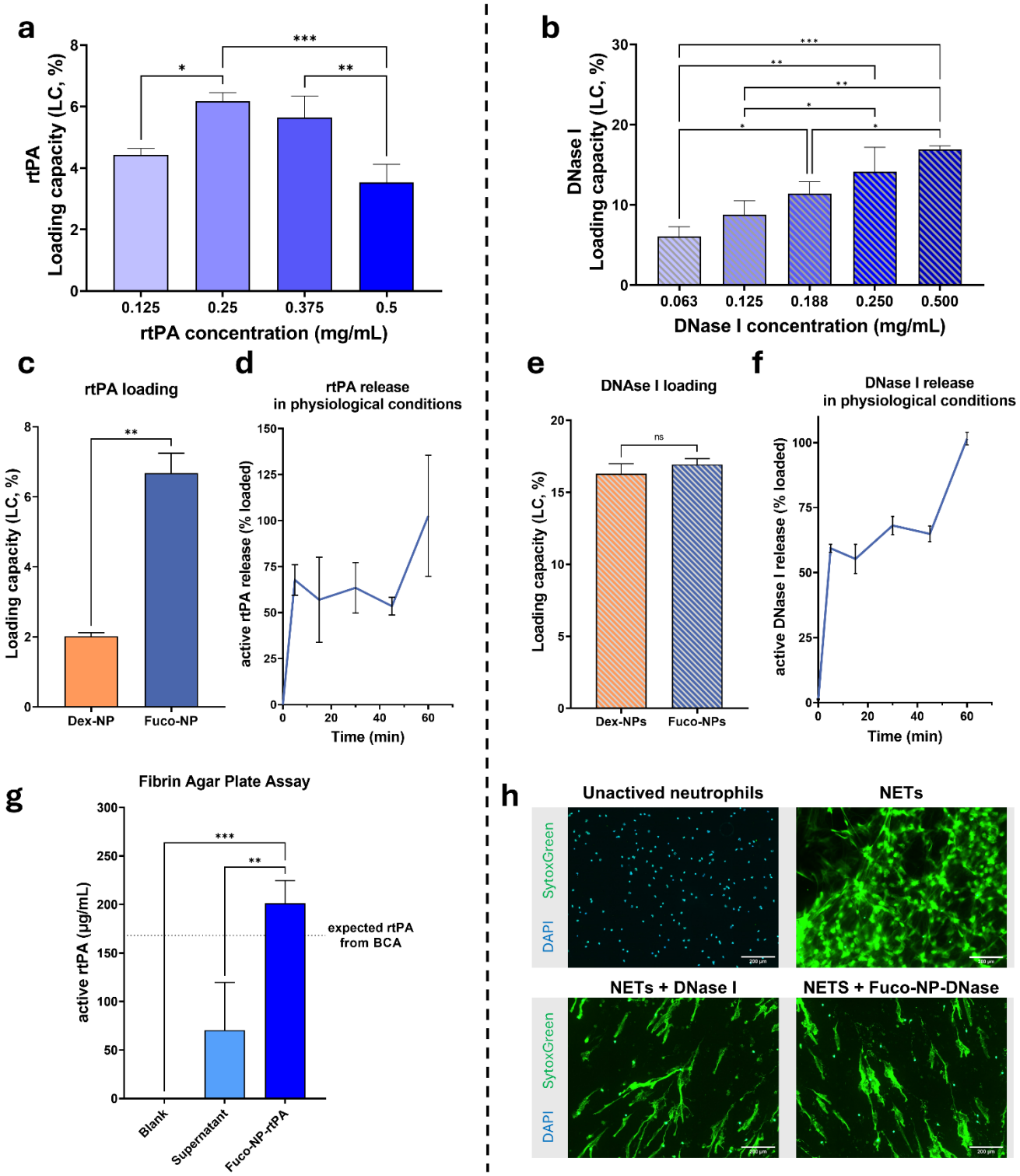

Figure 3. *Drug loading in NPs (rtPA, left column; DNase I, right column). (a) rtPA loading capacity in Fuco-NPs 2.5 mg/mL for various rtPA concentrations, measured by BCA (n = 3). (b) DNase I loading concentration in Fuco-NPs 2.5 mg/mL at pH = 3 for various DNase I concentrations, measured by BCA (n = 3). (c) Comparison of rtPA loading capacity in Dex-NPs and Fuco-NPs by BCA ([rtPA] = 0.25 mg/mL, [NP] = 2.5 mg/mL) (n = 3). (d) rtPA release in PBS at 37 °C with a dilution equivalent to 1 mg/kg in mice or 0.9 mg/kg in human measured by PefaFluor (n = 3). (e) Comparison of DNase I loading capacity in Dex-NPs and Fuco-NPs by BCA ([DNase I] = 0.5 mg/mL, [NP]=2.5 mg/mL) (n = 3). (f) DNase I release in PBS at 37 °C with a dilution equivalent to 5 mg/kg in mice measured by DNase I kit (n = 3). (g) FAPA determined concentration of active rtPA in Fuco-NP-rtPA and supernatant resulting from a loading experiment (n = 3). (h) NETolysis assay. Neutrophils isolated from human blood were seeded and then activated with PMA to release NETs, followed by treatment with DNase I or Fuco-NP-DNase. DAPI and SytoxGreen were used to differentially stain intra- and extracellular DNA. Top left: neutrophils not exposed to PMA and treatments. Top right: NETs released with PMA but treated with PBS. Bottom left and right: NETs released by PMA and treated with 0.5 mg/mL DNase I or equivalent DNase I concentration in Fuco-NP-DNase (experiment repeated three times) (scale bar = 200 µm).*

Aggregated platelets targeting

To validate the fucoidan-mediated targeting capacity of Fuco-NPs, a microfluidic setup was used to assess targeting to activated platelets in simulated blood circulation. Human blood is flown into collagen-coated microfluidic channels at arterial flow rates and the formation of platelet aggregates is observed in real-time. Various NP formulations were then flown into the channels before rinsing with PBS (see Sup.Fig.15.a and Sup.Movies 1-5). After rinsing, the fluorescence of NPs and platelets was measured (Fig.4.a). Their colocalization was then calculated with the Pearson's coefficient, as shown in Fig.4.b: Fuco-NPs demonstrated a statistically significant increase in colocalization with platelets when compared to Dex-NPs, as well as a global decrease in TRITC fluorescence (Fig.4.a) validating their targeting capacity. Furthermore, Fuco-NP-rtPA and Fuco-NP-DNase exhibited colocalization results similar to those of unloaded Fuco-NPs, proving that drug loading did not affect the targeting to aggregated platelets. It was also observed that Fuco-NPs had a superior colocalization to platelets than fucoidan-containing "classical" submicronic particles (Sup.Fig.15.b): this may stem from enhanced surface-to-volume ratio thanks to size reduction. Besides, this targeting was further quantified by *in vivo*

targeting of thrombi (Sup.Fig.15.c), validating the aggregated platelet targeting through P-selectin/fucoidan interaction to target thrombi.

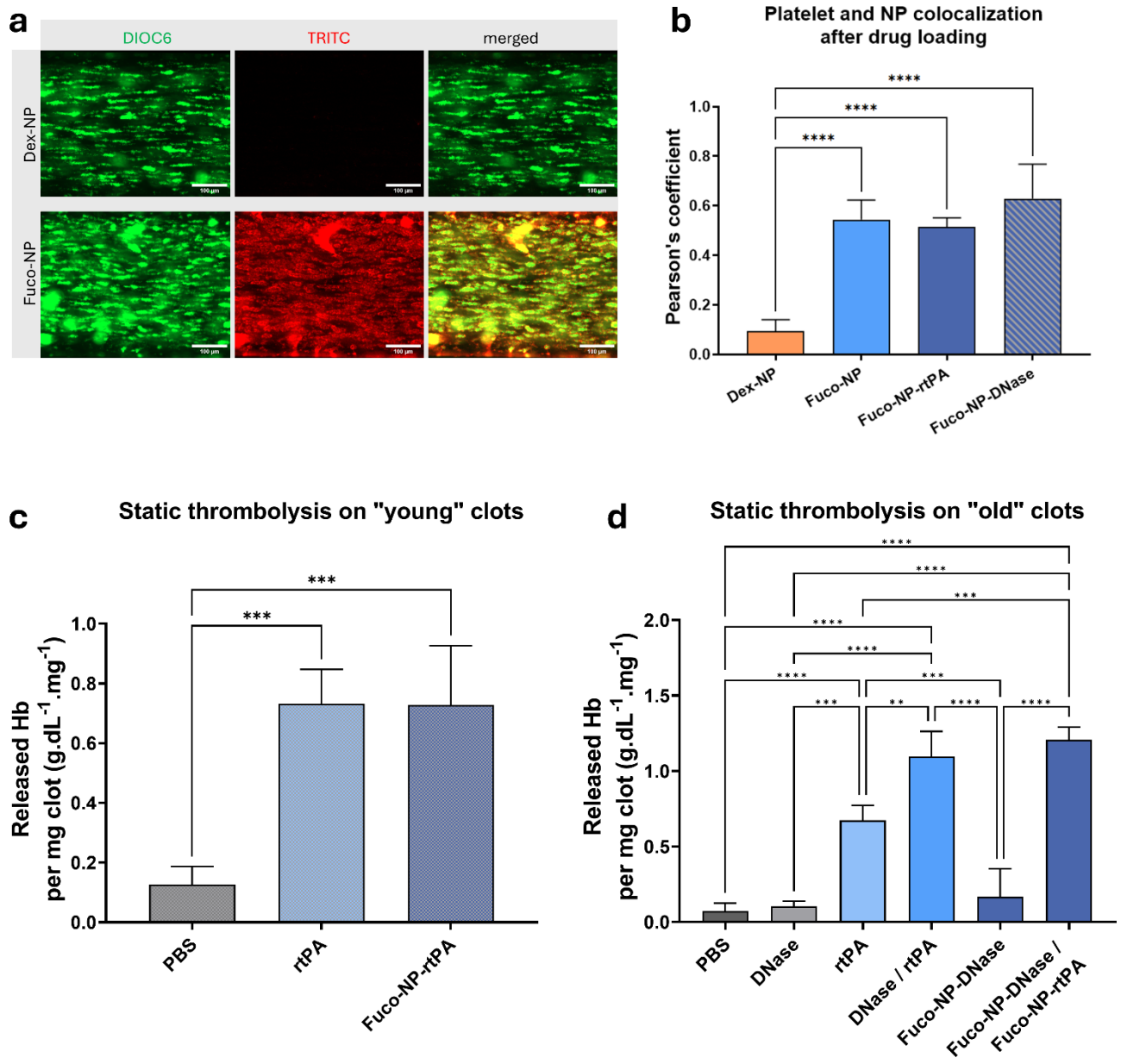

Figure 4. *Validation of targeting and thrombolytic properties. (a) Representative final images of the microfluidic targeting experiment on activated platelets. Aggregated platelets labeled with DIOC6 were obtained in microfluidic channels, and then 1 mg/mL TRITC-labeled Dex-NPs or Fuco-NPs were flown under arterial flow for 5 min, followed by 5 min rinsing with PBS (scale bar = 100 µm). (b) Resulting colocalization of TRITC and DIOC6 signal after rinsing, measured by Pearson's coefficient for 1 mg/mL Dex-NPs, Fuco-NPS, Fuco-NP-rtPA or Fuco-NP-DNase (n=4). Representative videos of targeting experiments are made available in the Supporting Information*

(in vitro targeting: Sup. Movies 1-4). (c) Static thrombolysis with "young" clots. "Young" clots were obtained after 60 min incubation of whole human blood with 10 mM $CaCl_2$ and 0.1 U/mL thrombin at 37 °C. After rinsing, they were weighted and treated with 1 µg/mL rtPA or Fuco-NP-rtPA at the equivalent rtPA dose. The released hemoglobin after 37 °C incubation for 1 h was quantified with the Drabkin's reagent and normalized to the initial clot mass (n = 4). (d) Static thrombolysis with "old" clots. "Old" clots were obtained after 24 h incubation of whole human blood with 10 mM $CaCl_2$ and 0.01 U/mL thrombin at 37 °C, then after rinsing they were weighted and treated with 1 µg/mL rtPA, 50 µg/mL DNase I, Fuco-NP-rtPA or Fuco-NP-DNase at the equivalent drug dose. The released hemoglobin after 37°C incubation for 1 h was quantified with the Drabkin's reagent and normalized to the initial clot mass (n = 4).

Static thrombolysis

Once Fuco-NP characterization, drug loading and targeting capacity were evaluated, static thrombolysis was assayed in static conditions on thrombi from human blood. The first formulation of *in vitro* clots, hereafter named "young" clots, were first created by mixing anticoagulated human whole blood with thrombin and $CaCl_2$ at 37 °C, and then they were incubated with rtPA or Fuco-NP-rtPA. The release of hemoglobin (Hb) and weight decrease were quantified, and the released Hb amount per mass unit of clot is reported. As can be seen in Fig.4.c, rtPA incubation at 1 µg/mL resulted in a significant release of hemoglobin (0.73 ± 0.12 $g.dL^{-1}.mg^{-1}$) when compared to control treatment (PBS, which was correlated with a clot weight reduction. Moreover, the Fuco-NP-rtPA, incubated at equivalent 1 µg/mL rtPA, produced a comparable thrombolysis as free rtPA with 0.73 ± 0.20 $g.dL^{-1}.mg^{-1}$ Hb released per mg of clot. Thus, Fuco-NP-rtPA retained the same activity as free rtPA in a static thrombolysis model. However, when considering the combo action of rtPA and DNase I, this model with "young" clots showed no difference between rtPA alone or rtPA combined with DNase I (Sup.Fig.16.a), even with different DNase I concentrations. This could be attributed to the possible absence of NETs in this static thrombus model since thrombi can have very different compositions.[2] A variation in the protocol for making *in vitro* clots from 1 h incubation to 24 h incubation, combined with a reduced concentration of thrombin, was tested, yielding clots that were named "old" clots. Based on the SytoxGreen/DAPI differential staining of extracellular and nuclear DNA, "young" and "old" clots were stained and the total fluorescence ratio of SytoxGreen over DAPI was quantified: a significant increase in the SytoxGreen and DAPI mean

fluorescence intensity ratio from 1.06 ± 0.01 to 1.30 ± 0.05 was observed, indicating that "old" clots contained more extracellular DNA than "young" ones (Sup.Fig.16.b), likely due to increased NET formation. The thrombolysis experiment was repeated to evaluate DNase potentiating action on rtPA on these "old" clots, now comparing rtPA at 1 µg/mL, DNase I at 50 µg/mL and equivalent drug concentrations of Fuco-NP-rtPA and Fuco-NP-DNase (Fig.4.d). In this model, rtPA alone amounted to 0.67 ± 0.10 $g.dL^{-1}.mg^{-1}$ Hb released per mg of clot, while rtPA and DNase free drugs combo achieved 1.10 ± 0.17 $g.dL^{-1}.mg^{-1}$ released Hb per mg clot, thus demonstrating a statistically significant increase in thrombolysis for the rtPA + DNase I combo, while DNase I alone was no different than the control treatment (PBS). Furthermore, the combo of Fuco-NP-rtPA and Fuco-NP-DNase resulted in 1.21 ± 0.08 $g.dL^{-1}.mg^{-1}$ released Hb per mg clot, similar to the free drugs combo, and significantly superior to the rtPA alone condition. Histological analysis revealed no structural differences in thrombi after the different treatments (Sup.Fig.17). This experiment reflected that like clinical thrombi,[41] artificial thrombi could vary in composition, including NET formation; but for NET-containing thrombi, DNase I (ineffective alone) can improve thrombolysis with rtPA and that Fuco-NP-rtPA and Fuco-NP-DNase are viable formulations for delivering these active drugs.

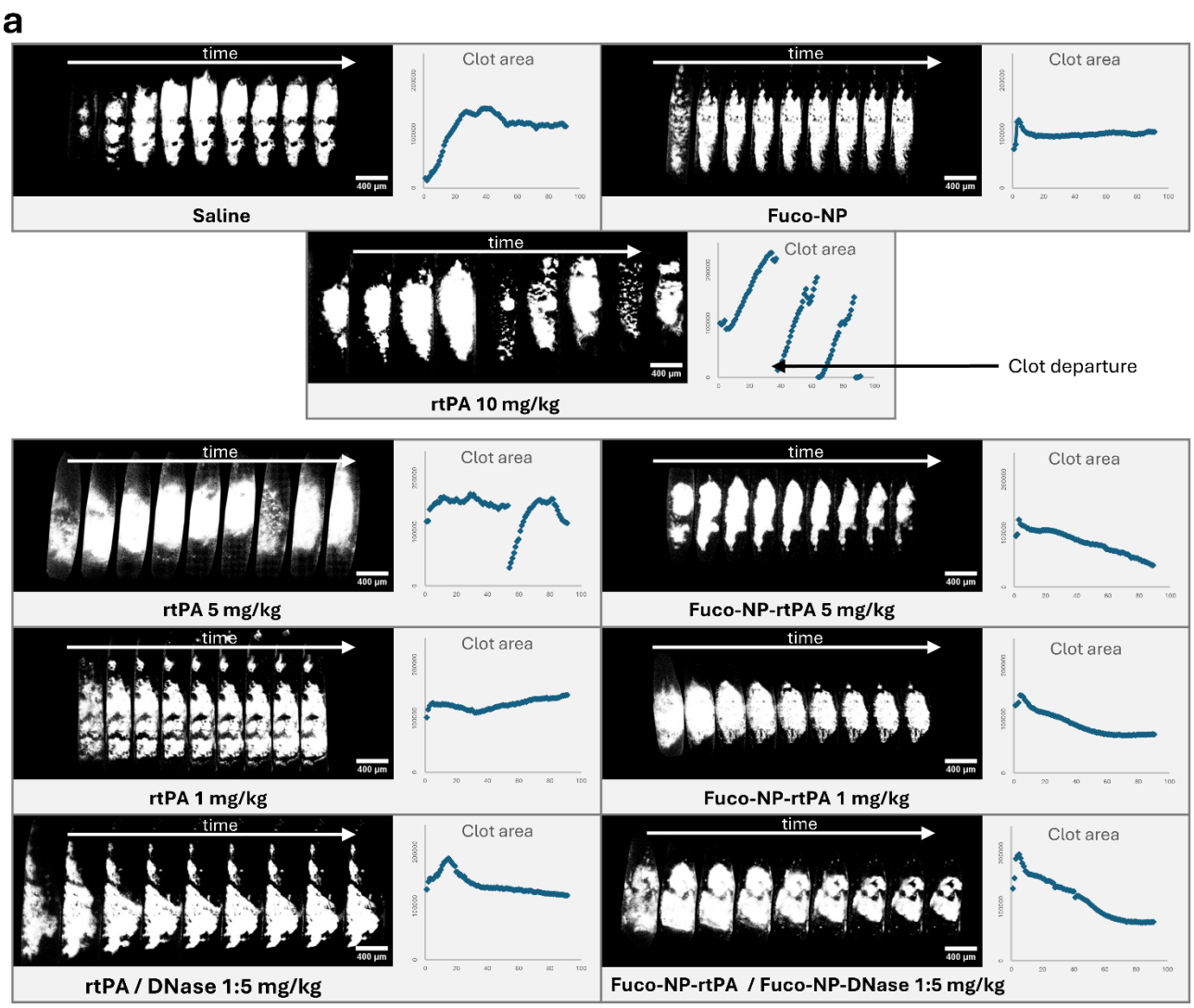
a
time
Clot area
400 µm
Saline
Fuco-NP
rtPA 10 mg/kg
Clot departure
rtPA 5 mg/kg
Fuco-NP-rtPA 5 mg/kg
rtPA 1 mg/kg
Fuco-NP-rtPA 1 mg/kg
rtPA / DNase 1:5 mg/kg
Fuco-NP-rtPA / Fuco-NP-DNase 1:5 mg/kg

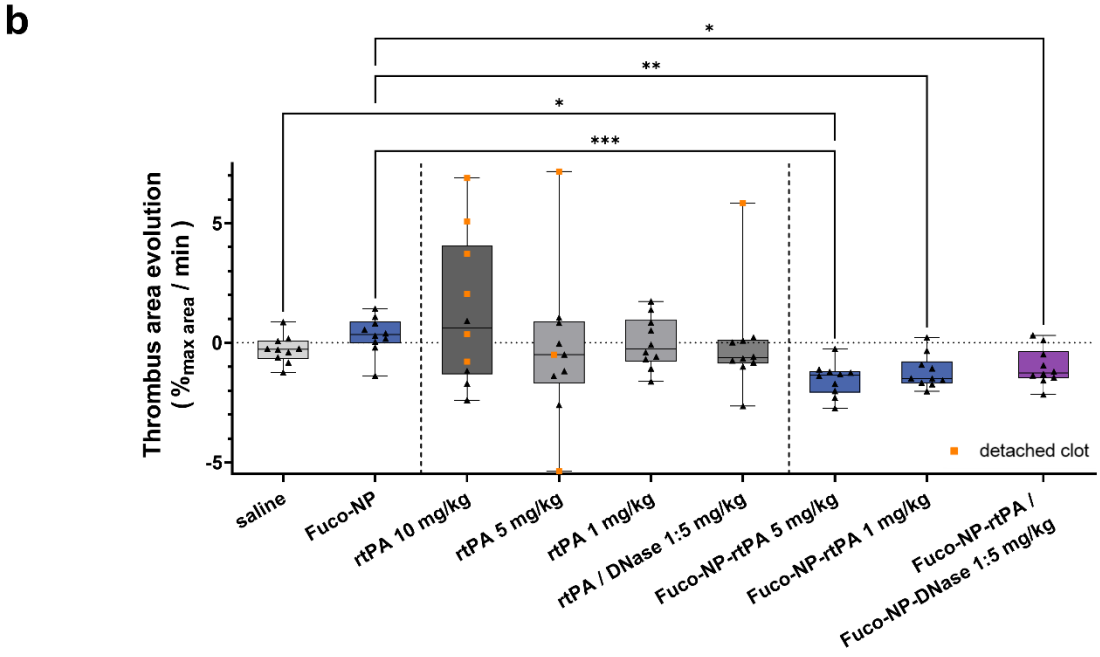
b
Thrombus area evolution
(%max area / min)
5
0
-5
*
**
*
***
detached clot
saline
Fuco-NP
rtPA 10 mg/kg
rtPA 5 mg/kg
rtPA 1 mg/kg
rtPA / DNase 1:5 mg/kg
Fuco-NP-rtPA 5 mg/kg
Fuco-NP-rtPA 1 mg/kg
Fuco-NP-rtPA /
Fuco-NP-DNase 1:5 mg/kg

Figure 5. *In vivo thrombolysis in the FeCl3 mesenteric vein model. (a) Representative thrombi evolutions over time. Each thrombolysis experiment lasted 30 min, and the mosaics shown here are composed of juxtaposed thrombi binary masks acquired every 3 min. On the right of each mosaic is drawn to the corresponding area evolution curve over 30 min. The top three thrombi correspond to controls (saline, empty Fuco-NPs and rtPA 10 mg/kg) (scale bar = 400 µm). (b) In vivo thrombus area evolution over various treatments, represented as boxes and whiskers. Boxes are delimited by 25% and 75% quartiles and whiskers delimit minimum and maximum values. Detached clots are marked with orange squares. Statistical analysis was performed with one-way Welch's ANOVA with Dunnett's T3 multiple comparison test (n = 10).*

In vivo thrombolysis

The *in vivo* thrombosis model was performed as described in Sup.Fig.18 with a murine mesenteric vein $FeCl_3$ thrombosis, with male (24.9 ± 2.3 g weight) and female (19.9 ± 2.4 g weight) mice. Once the thrombus formation was observed by intravital macroscopy through platelet aggregation, the samples were injected into the retro-orbital vein and continuous imaging was performed for 30 min (Sup. Movies 6-15). The thrombus area was measured over time, and the rate of thrombus degradation was calculated to account for disparities in the thrombi area. Each treatment group contained 10 animals, with equipartition of male and female mice. Saline and empty Fuco-NP (equivalent NP concentration to the Fuco-NP-rtPA 5 mg/kg) were used as negative control treatments, while the 10 mg/kg rtPA injected as a free drug served as the positive control as established before for murine models.[38] Fuco-NPs loaded with rtPA alone at 5 mg/kg or 1 mg/kg were compared to free rtPA at the same concentration. The potential synergic effects of DNase I with rtPA were also investigated, with their co-injection as well as the co-injection of Fuco-NP-rtPA 1 mg/kg with Fuco-NP-DNase 5 mg/kg. Representative clot evolutions over time are shown in Fig.5.a after treatment injection, with the respective clot area evolution curves (on the right of each clot). First, the saline treatment demonstrated that the thrombus keeps growing for a few minutes before reaching a maximum area before stabilizing. Empty Fuco-NP treatment also resulted in a stable clot. However, when treated with rtPA 10 mg/kg, the thrombi either diminished in size, or showed important remodeling, sometimes followed by clot departure, where the clot is visibly detached whole from the vessel and carried away. These results were recapitulated in Fig.5.b displaying the thrombi area evolution: while saline and empty Fuco-NP treatments

resulted in stable clots (respectively -0.29 ± 0.57%.min^{-1} and 0.32 ± 0.77%.min^{-1}), six out of ten clots treated with rtPA 10 mg/kg were detached (n = 6, evolution of 2.98 ± 2.82%.min^{-1}), and the four remaining displayed decreasing clots (n = 4, evolution of -1.24 ± 1.17%.min^{-1}). Diminishing the rtPA concentration reduced how affected the thrombi were: at 5 mg/kg only three clot departures and the seven remaining displaying clot area evolutions of -0.55 ± 1.30%.min^{-1} in average, while rtPA treatment at 1 mg/kg resulted in stable clots (evolution of -0.00 ± 1.09%.min^{-1}). Interestingly, this might shed light on a major limitation of rtPA-based clinical treatment of stroke: a low rate of recanalization, and significantly decreased recanalization when the elapsed time from stroke onset to treatment increases, as explicit in the American guidelines for stroke treatment: “benefit of therapy is time dependent, and treatment should be initiated as quickly as possible”.[42,43] This could indicate that fibrinolysis does not equal thrombolysis, as is often mistakenly perceived. Some clots, for instance, during the early AIS phase, might be more susceptible to rtPA as they are still developing. Another limitation might reside in the rtPA mechanism of action by binding to fibrin which could inherently limit its action in the clot;[44] this was also investigated by Bannish *et al*., 2017, who explored how rtPA-mediated fibrinolysis proceeded as a moving front through the clot.[45] It could explain an activity of rtPA limited to the edges or leading edge of a thrombus, thus elucidating its below-ideal efficacy and even why clot departures were seen, eroded from the edges but not destroyed. Most notably, such departed clots are still problematic and could form further emboli in distal vessels, even if often counted as successful events in *in vivo* studies, which therefore ignore the problematic secondary emboli. Regarding rtPA loaded NPs, only Fuco-NP-rtPA 5 mg/kg showed statistically significant improvement (evolution of -1.54 ± 0.69%.min^{-1}) compared to both saline and empty Fuco-NP treatment, with a similar degradation rate to free rtPA 10 mg/kg (undetached clots). As for Fuco-NP-rtPA 1 mg/kg (evolution of -1.21 ± 0.70%.min^{-1}), it also resulted in a comparable thrombus degradation to free rtPA 10 mg/kg (undetached clots), significantly better than empty Fuco-NPs. To study the combo treatment, the lowest rtPA concentration (1 mg/kg) was chosen and combined with DNase I at 5 mg/kg. One clot out of ten departed, and the other displayed relatively stable clots (n = 9, evolution of -0.69 ± 0.86%.min^{-1}). When Fuco-NP-rtPA and Fuco-NP-DNase were co-injected at equivalent drug concentrations, the size of the thrombi decreased (evolution of -1.01 ± 0.77%.min^{-1}) but without

improvement over rtPA alone or Fuco-NP-rtPA treatments. Thrombus area evolutions quantified without the departed clots are shown in Sup.Fig.19. This demonstrated a benefit in using Fuco-NP-rtPA compared to free rtPA: systematic clot reduction was observed, and the lowering of the rtPA concentration used could reduce associated side effects. While this behavior is not fully understood, the absence of an improved thrombolytic capacity of Fuco-NP-rtPA in static *in vitro* experiments (Fig.4) tends to indicate a targeting-related behavior or an unknown *in vivo* biological effect which could only be observed in the *in vivo* experiment. It can be hypothesized that a sustained release over time by Fuco-NPs, attached to the clot, could be more beneficial mechanistically than free rtPA, which could be inhibited faster or lack the improved accumulation imbued by Fuco-NP targeting. As for the potentiating effect of DNase I or Fuco-NP-DNase on thrombolysis, no synergistic effect was observed. The concentrations used were 1 mg/mL rtPA (minimum where Fuco-NP-rtPA showed an effect but where free rtPA was not efficient) with DNase 5 mg/kg (highest dose possible with the constraint of using DNase I formulated at 1 mg/mL). This indicated that the $FeCl_3$ thrombotic model, which was very relevant to measure Fuco-NP-rtPA-mediated thrombolysis and to observe the mechanistic differences between free and loaded rtPA, may not be adequate to investigate NET-dependent synergies.

Biodistribution

Fuco-NP accumulation at the thrombus site is clear from *in vivo* acquisition and was quantified with the targeting measurements *in vivo* (Sup.Fig.15.c and Sup. Movies 6-15). Nonetheless, NP fate in living organisms is critical. Therefore, four organs known to be involved in NP circulation removal (liver, spleen, kidney, and lung) were harvested at the end of the *in vivo* thrombolysis experiments for the saline and Fuco-NP treatment. In addition to the classical HES coloration, Alcian Blue (AB) coloration was performed to specifically stain acidic polysaccharides, such as glycosaminoglycans or mucopolysaccharides, but not chromatin DNA.[30] Representative organ histological slices are shown in Fig.6.a. First, based on HES coloration no pathological changes were apparent between animals treated with saline or with Fuco-NPs. Regarding AB coloration, while some blue staining occurred in untreated organs, especially in the kidneys, differential staining was obvious after treatment with Fuco-NPs, especially in the liver or the spleen. Based on this differential staining, biodistribution of the Fuco-NPs in the

selected organs could be inferred, as determined in Fig.6.b. Increased Fuco-NP presence was evidenced in the liver, spleen, and lung with statistical significance (respectively 8-fold increase, 11-fold increase, and 4-fold increase over saline treatment), while no difference could be noted in the kidney. CD68 staining was also performed to compare macrophages localization (Sup.Fig.20). Notably, the presence of Fuco-NPs in the various organs followed specific patterns, as seen at lower magnification in Sup.Fig.21. More precisely, the presence of Fuco-NPs in liver was evidenced in tens of micrometers-sized cellular or sinusoidal shaped areas, homogeneously distributed throughout the organ, following similar patterns as macrophages. In the spleen, Fuco-NPs were localized in specific ring-shaped areas surrounding the lymphoid white pulp, resembling the marginal zone. On the contrary, macrophages were present throughout the red pulp. In the kidney, AB staining was similar in control animals and in Fuco-NP treated animals, corresponding to glomeruli and showing no increased AB signal between controls and Fuco-NP treated mice, with few macrophages present. In the lung, some staining was evident in the control treated animals, most likely due to the presence of mucosal polysaccharides, but it was strongly enhanced with Fuco-NP treatment, arranged in tens of micrometer-sized cellular shaped areas throughout the whole organ, and following similar patterns as macrophages. The organ distribution is coherent for 315 nm NPs: absence from the kidneys, but evidenced in the liver, spleen, and lungs with distribution patterns coherent with macrophages; however, specific accumulation of Fuco-NPs in the marginal zone of white pulp in the spleen could be seen.[46] This marginal zone is instrumental in building specific responses to the phagocytosis-mediated activation of certain cell types. All these elements point toward a mononuclear phagocyte system (MPS)-dependent processing pathway.[46,47] Interestingly, dextran-based materials can be degraded in the human body, notably in the liver and spleen: enzymes capable of hydrolyzing dextrans, by (1 → 6)-α-D-glucosidase activity, were found in animal and human tissues,[48–50] and the *in vitro* biodegradation assay of Sup.Fig.9 indicated that such an enzyme could effectively degrade Fuco-NPs. The presence of phosphate diester bonds, which could hinder this process, may also be hydrolyzed in physiological conditions.[50] Nonetheless, future experimentation on long-term biodegradation and clearance of Fuco-NPs will be necessary. Finally, healthy mice were treated with Fuco-NPs at a concentration equivalent to 1 mg/kg rtPA delivery in humans, and the inflammatory profile was

measured after 1, 3, and 24 h with the following cytokines: GM-CSF, IFN-γ, IL-1β, IL-2, IL-4, IL-5, IL-10, and TNF-α. GM-CSF, IL-2 and IL-5 were undetectable in all groups and the other cytokine levels are shown in Sup.Fig.22, demonstrating a very low inflammatory response (slight IFN-γ increase, and transient TNF-α increase concomitant to an anti-inflammatory IL-10, while the pro-inflammatory IL-1β remained low). While extensive *in vivo* safety studies would need to be conducted before clinical use could be envisioned, this suggested that the Fuco-NP administration was well tolerated at the inflammatory level.

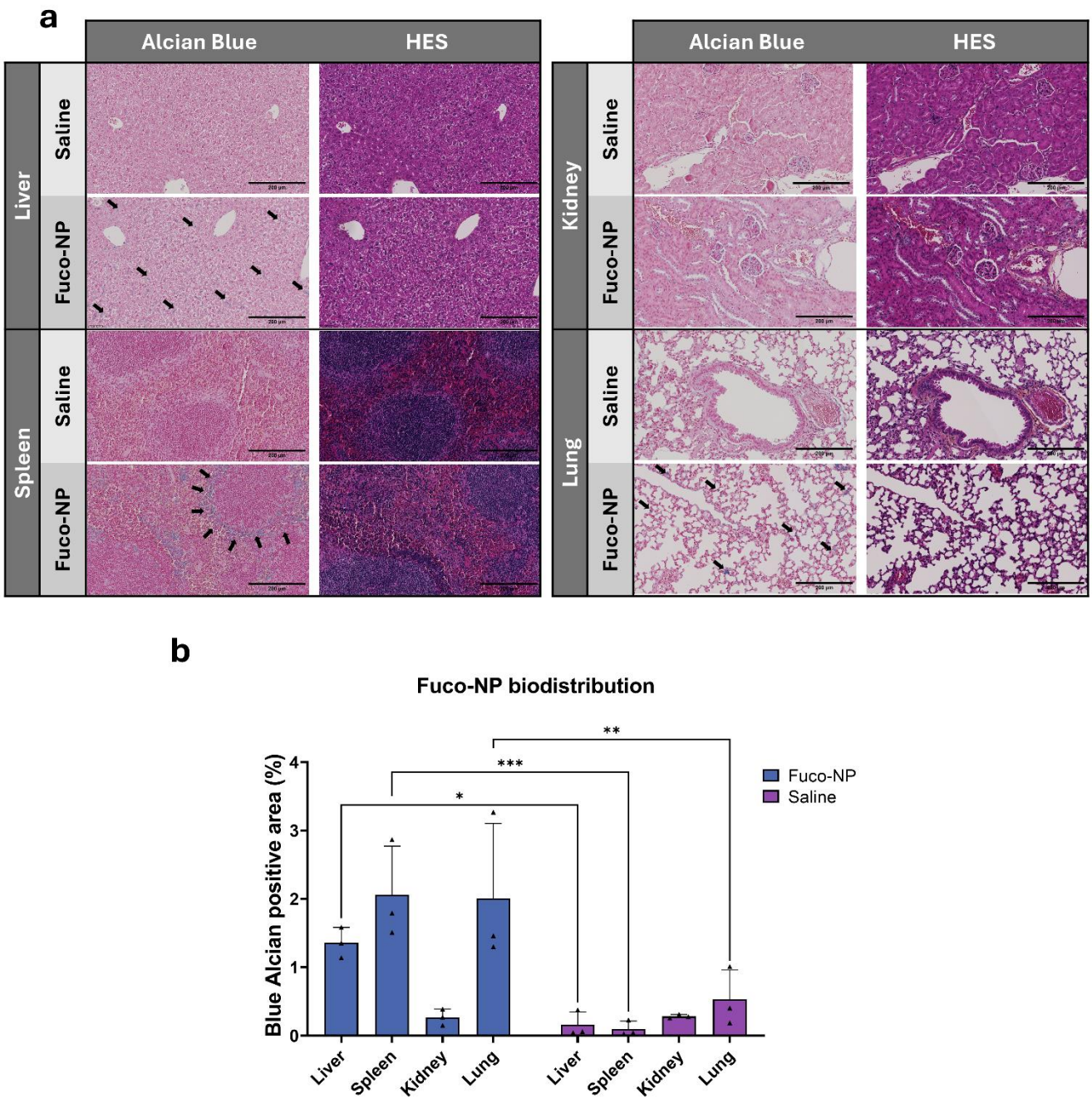

Figure 6. *Biodistribution of Fuco-NPs in mice after thrombosis experiment. Three animals were used for saline or Fuco-NP treatment each. AB and HES colorations were obtained for liver, spleen, kidney, and lung for each animal. (a) Representative images from different organs of animals treated with saline or Fuco-NP (representative Fuco-NP staining was indicated by black arrows). All slices shown on one line come from the same animal and were aligned (scale bar = 200 µm). (b) Quantification of AB positive coloration in each organ for the Fuco-NP (blue) or saline (purple) treatment. The total area stained blue was measured for each entire organ slice and*

divided by the total organ area. A two-way ANOVA was performed, with Tukey's multiple comparison test to compare only the differences per organ (n = 3).

Conclusions

In this study, we present full polysaccharide NPs that could be used for targeted thrombolytic treatment. These were designed with a simple and robust protocol which was developed with the help of a valuable microemulsion theoretical framework, which allowed a significant size reduction and synthesis robustness for a protocol initially designed for microparticle synthesis.[29,30] The resulting 315 nm NPs fell in the desired size window of 150-400 nm to remain in the circulation, and were fully characterized, including good stability and freeze-drying capacities, which are especially interesting for future developments. Their biocompatibility and safety were assessed *in vitro* with cytotoxicity and hemolysis assays, and explored *in vivo* with biodistribution in the liver, spleen, kidney, and lung. They demonstrated their ability to specifically accumulate at the thrombi site *in vivo* through fucoidan targeting of P-selectin on activated platelets. Furthermore, the loading of rtPA and DNase I by adsorption was successfully optimized and ensured that enzymatic and thrombolytic activities were retained after loading, which was demonstrated *in vitro* on artificial thrombi while validating that DNase I could potentiate rtPA action on certain blood clots. Besides, qualifying the action of Fuco-NP-rtPA and Fuco-NP-DNase over various subtypes of thrombi, would eventually help pinpoint which combinations would be best suited for different thrombotic pathologies, and thus potentially help improve the standard of care for patients. *In vivo,* efficient thrombolysis of Fuco-NP-rtPA was demonstrated at 50 and 10% of the recommended free rtPA dose in mice, despite Fuco-NP-DNase not providing thrombolysis improvement in this model. Strikingly, this improved Fuco-NP-rtPA-mediated thrombolysis was accompanied by a systematic *in situ* clot reduction instead of having clot detachments as was the case with the free rtPA. Future development of these Fuco-NPs should include scaled-up production in a GMP setting, and a more complete *in vivo* exploration of their behavior and clearance in living organisms, validating the absence of toxicity and the safety improvement by working with these formulations. The *in vivo* degradability of these materials should also be assessed. Furthermore, P-selectin is expressed by both activated platelets and activated endothelium, and the precise role of each cell type in the

targeting of the thrombus localization may need to be assessed in future studies. The microemulsion-based approach is especially interesting as it led to enhanced storage stability (including freeze-drying capacity) and critical size reduction of polymeric hydrogel NPs. The implementation of this concept over various protocols might improve robustness and ease the design of emulsion-involving synthesis. Finally, these Fuco-NPs, which could be loaded with rtPA or other drugs, show promising results toward application for thrombotic diseases.

Materials and Methods

Materials: Dextran 40 kDa was purchased from Pharmacosmos (Holbæk, Denmark, #5510 0040 1007); FITC-Dextran 40 kDa and TRITC-Dextran 40 kDa were purchased from TDB Consultancy (Uppsala, Sweden, #FD40 and #TD40). Fucoidan (M_n = 18 kDa / M_w = 104 kDa) was a gift from Algues & Mer (Ouessant, France, #MMWFSA14093). Vegetable sunflower oil (Lesieur - Huile Coeur de Tournesol, Lesieur S.A.S, Asnieres-sur-Seine, France) was purchased from a local supermarket (Monoprix, Paris, France). Polyglycerol polyricinoleate (PGPR) was kindly supplied by Palsgaard (Lyon, France, # PGPR 4150). Fetal bovine serum (FBS) was purchased from Pan-Biotech (Aidenbach, Germany, #P30-3306). HUVEC cell line (ATCC, Manassas, Virginie, #ATCC-CRL-1730) was used at fewer than 40 passages. Tween 80 (#P1754), Trisodium trimetaphosphate (STMP, #T5508), Sodium Dodecyl Sulfate (SDS, #L3771), Sucrose (#S7903), fibrinogen type I from human plasma (#F3879), thrombin from human plasma (#T7009), plasminogen from human plasma (#528175), Phorbol 12-myristate 13-acetate (PMA, # P8139-5MG), Iron (III) Chloreide hexadydrate ($FeCl_3$, # 236489-100G), Dextranase (#D0443) were purchased from Sigma Aldrich (Saint-Quentin-Fallavier, France). DMEM, low glucose, pyruvate (#31885049), Antibiotic Antimycotic solution (#15240062), PBS 1X and 10X (#14040133 and #14080055), Rhodamine phalloidin (#R415), low melting point agarose (#R0801), DIOC6 (D273), DAPI (#62247), SytoxGreen (#S7020) were purchased from Thermo Fisher Scientific (Massachusetts, United States). Horm collagen type I was purchased from Takeda Pharmaceutical (Tokyo, Japan). rtPA (alteplase) was purchased from Boehringer Ingelheim (Ingelheim am Rhein, Germany, # Actilyse). DNase I (dornase alfa) was purchased from Roche – Genentech (San Francisco, United States, #Pulmozyme 2500 U/2,5 mL). The PefaFluor kit

(#CG8433) for rtPA titration was purchased from Interchim (Montluçon, France). The DNase I detection kit (#JE-PP-410L) was purchased from Euromedex (Souffelweyersheim, France). Polymorphprep (#1114683) was purchased from Proteogenix (Schiltigheim, France). Anti-H3 (#ab5103), anti-MPO (#ab90810), anti-CD68 (#ab283654) antibodies, and IHC detection kit (#ab236468) were purchased from Abcam (Amsterdam, Netherlands). Human whole blood was acquired from EFS (Bichat Hospital, Paris, France), the French blood donation institute, under a research convention, in fePPACK, sodium citrate or EDTA collection tubes.

Nanoparticle synthesis: Polysaccharide nanoparticles (NPs) were obtained through a water-in-oil (w/o) microemulsion, with chemical crosslinking in the aqueous phase. A polysaccharide solution (300 g/L dextran, 6 M NaCl) was prepared; for fluorescent NPs, a 5:95 mass mixture of TRITC-Dextran 40 or FITC-Dextran 40 with Dextran 40 was used. For targeting NPs, fucoidan was substituted to dextran at a 10 wt.% ratio. 15 mL of organic phase composed of sunflower oil and 6 wt.% surfactant (60:40 PGPR and Tween 80) was cooled at -20°C for 30 min. Meanwhile, 1200 mg of the polysaccharide solution is mixed with 60 µL of 10 M NaOH for 10 min. 240 µL of 30 wt.% STMP solution was added before quick mixing for 1 min. 600 µL of this aqueous mix was then added dropwise to the organic phase under dispersion with a stand-disperser (Polytron PT 3100, dispersing aggregate PT-DA 07/2 EC-B101, Kinematica, Luzern, Switzerland) for 2 min 30 s at 30 000 rpm on ice. The resulting emulsion was incubated at 50°C for 20 min before successive purification by ultracentrifugation (50 000 g, 30 min): the pellets were resuspended first with SDS 0.04 wt.% four times, then with ultrapure water three times. The resulting NPs were stored at 4°C in ultrapure water. Further concentrating of NPs could be performed with ultracentrifugation devices with size cutoff of 300 000 Da (Vivaspin, Dutscher, Issy-les-Moulineaux, France). Stable freeze-dried NPs were obtained with the LyoVac GT2 freeze dryer (SRK Systemtechnik, Riedstadt, Allemagne) after -80 °C freezing for 1 h in a 1 wt.% sucrose solution. Submicroparticles (SPs) for comparison were synthesized as per Zenych et al., 2021.[30]

HLD screening: HLD screenings were performed by mixing surfactants together for a total of 90 mg in centrifuge tubes, then adding oil phase (750 µL sunflower oil) with agitation for 1 h. Then water phase is then added (750 µL ultrapure water, saline solutions, or aqueous phase from the NP synthesis) slowly. A gentle agitation by three

up-and-down inversions is performed then the tubes are left to incubate at RT for more than 1 h, before they are observed and photographed. Surfactant gradients were used to determine unknown parameters as described by Abbott [32]: two known surfactants (Tween 80 and Span 80) were used to determine sunflower oil EACN, then Tween 80 with PGPR in sunflower oil were used to determine PGPR Cc. HLD was found to be independent of salinity for PGPR. Constants used: k = 0.16, F(S) = 0.13*S, and α was ignored by working at 25°C (RT). Known values were: $Cc_{Tween80}$ = -3.7, Cc_{Span80} = 3.1. Determined values were: Cc_{PGPR} = 4, $EACN_{sunflower\ oil}$ = 16.

Physico-chemical characterization: The NPs formulations were studied for particle morphology, size and zeta potential distributions, mass concentration, and elemental composition. Particle morphology was visualized by Transmission Electron Microscopy (TEM) (Philips FEI Tecnai 12, Amsterdam, Netherlands), negatively stained with 1 wt.% uranyl acetate for 5 min. Hydrodynamic size (diameter), polydispersity (PDI) and Zeta potential (ζ-potential) were measured by Dynamic Light Scattering (DLS) and Electrophoretic Light Scattering (ELS), respectively (Zetasizer Nano ZS, Malvern Instruments, Orsay, France). Samples were diluted in distilled water, 0.9 wt.% NaCl or PBS 1X for size, and in 1 mM KCl for ζ-potential determination. All runs were performed at 25°C in triplicate. Mass concentration (yield) was determined by freeze-drying. Elemental composition was assessed by total reflection X-ray fluorescence spectroscopy (TXRF) technique to quantify the phosphorus and sulfur content (S2 PICOFOX Bruker, Massachusetts, United States). Fourier transform infrared spectroscopy (FTIR) spectra were obtained after drying and inclusion in KBr pellets (Thermo Nicolet AVATAR 370 FTIR spectrometer, Thermo Electron Corporation, Waltham, MA). The stability of Fuco-NPs and compared SPs in various solvents (ultrapure water, 0.9 wt.% NaCl, PBS 1X) was evaluated 6 h after solvent exchange, or after various timepoints at 37°C by DLS. For long-term storage stability, some batches were kept in storage at 4°C for up to 13 months.

Fucoidan and phosphate chemical quantification: The fucoidan content of NPs was determined by a semiquantitative solid-phase colorimetric assay for sulfate titration [51]. Briefly, 12.5 µg of Fuco-NPs in suspension at a concentration of around 1 mg/mL were added by 5 µL drops on a piece of Whatman Chromatography paper grade 1 with drying between each drop addition. The paper was first soaked into a methanol/acetone (6:4)

solution for 3 min and then into a methanol/acetone/water (6:4:15) solution with 50 mM HCl and 0.1 wt.% methylene blue for 10 min. Finally, the paper was extensively washed with acetic acid/methanol/acetone/water (5:6:4:85) until no coloration was detected in the washing solution. The paper was then transferred to the Eppendorf, containing 0.5 mL methanol with 2 wt.% SDS, and incubated for 15 min at 50°C. A 0.2 mL portion of the extracted dye was placed in a 96-well plate, and its concentration was determined by reading absorbance at 663 nm with a Varioskan LUX multiplate reader (Thermo Fisher Scientific, Massachusetts, United States). Standard curves were obtained from fucoidan in solution with known concentrations. The phosphate content of NPs was determined by a colorimetric assay. Briefly, two solutions A (2.5 g/L ammonium metavanadate NH_4VO_3, 13 wt.% HNO_3) and B (5 g/L ammonium heptamolybdate $(NH_4)_6Mo_7O_{24}$) are prepared. 1 mL of around 1 g/L NPs are incubated with 1 mL HNO_3 10 wt.% for 3 h at 105°C, then 0.4 mL HNO_3 65 wt.%, 2 mL solution A, 2 mL solution B and 3.6 mL water are added. After 15 min incubation at room temperature (RT), the concentration was determined by reading absorbance at 405 nm. Standard curves were obtained from H_3PO_4 solutions with known concentrations.

Biodegradation *in vitro* assay: To evaluate the biodegradability of the polysaccharide nanoparticles, fluorescent TRITC-Fuco-NPs (1 mg/mL) were incubated in 1% (v/v) dextranase in PBS 1X (200 µL) or PBS 1X for 1 h at 37°C. The samples were then ultracentrifuged for 15 min at 50 000G, and the pellet were resuspended in 200 µL ultrapure water. The total TRITC fluorescence of the supernatants and resuspended pellets was measured with a Varioskan LUX multiplate reader (Thermo Fisher Scientific, Massachusetts, United States). Furthermore, DLS measurements were performed on the supernatants and resuspended pellets.

Cell culture and cytotoxicity assay: To evaluate the cytotoxicity of the NPs, a resazurin Fluorometric Cell Viability Assay (#TOX-8 kit) was used on confluent Human Umbilical Vein Endothelial Cells (HUVECs). The cells were cultured in low glucose DMEM supplemented with 10 % v/v FBS and 1 % v/v antibiotic-antimycotic; the cells were kept in an incubator at 37°C in a humidified atmosphere of 5% CO_2. Cells were seeded into 96-well plates with 30 000 cells per well. Following 24 h of incubation, the medium was changed to Fuco-NPs resuspended in culture medium in a range of 0.1 to 1 g/L, and the cells were cultured for another 24 h. Cells cultured with equivalent PBS 1X medium

dilution were set as control. Negative controls were culture medium only, and positive controls were 1 % (v/v) Triton X-100 in culture medium for 15 min. Then the medium was replaced with 100 µL 10 % (v/v) Resazurin solution in culture medium, and the plates were covered in foil and incubated for another 2 h. The Resazurin absorbance signals were monitored at 570 and 590 nm wavelengths with a Varioskan LUX multiplate reader (Thermo Fisher Scientific, Massachusetts, United States). The corrected absorbance values were blank corrected: $A' = A_{570nm} - A_{590nm}$, and the relative cell viability was expressed as $(A' - A'_{neg}) / (A'_{pos} - A'_{neg}) \times 100\%$, with the negative and positive control absorbances respectively averaged in the control wells as detailed above. To examine possible cell morphology changes after co-incubation with Fuco-NPs, HUVECs cells were seeded in 8-wells Lab-Tek II Chamber Slide (Thermo Fischer Scientific, Massachusetts, United States) with 10 000 cells per well. The medium was changed 24 h to Fuco-NPs resuspended in culture medium in a range of 0.1 to 1 g/L, and the cells were cultured for another 24 h. Cells cultured with equivalent PBS 1X medium dilution were set as control. Next, cells were fixed with 4% (v/v) paraformaldehyde for 30 min at 4°C. After rinsing with PBS, cells were permeabilized with Triton X-100 0.1 wt.% in PBS for 5 min at RT then washed twice with PBS before incubation for 60 min at RT with 1% (v/v) Phalloidin-Rhodamine in PBS. After two PBS washes, the slides are mounted with a Mounting Medium with DAPI. Visualization was performed with a confocal microscope (Zeiss LSM 780, Iena, Germany).

Hemolysis assay: To evaluate hemolysis, human whole blood was collected in EDTA tubes, then centrifugated at 500 G for 5 min. After plasma removal, an equivalent volume of saline was added. Centrifugation and saline addition were repeated. After a third centrifugation with PBS addition instead of saline, the RBCs suspension was then diluted to 1/50 in PBS. After visual verification (turbidity, sedimentation), 1 volume of samples was mixed to 19 volumes of diluted RBCs in V-bottom 96-well plates. For negative and positive controls, PBS and 20 % (v/v) Triton X-100 were respectively used. After 60 min incubation at 37°C with slow agitation, the plate was centrifuged for 5 min at 500 G, then the supernatants were collected, and the absorbance is read at 541 nm.

Blood margination: An *in vitro* blood flow assay was performed to evaluate the margination of NPs within blood flow. Micro-channels of Vena8 Fluoro+ chambers (width: 0.04 cm, height: 0.01 cm, and length: 2.8 cm; Cellix Ltd, Dublin, Ireland) were rinsed with

NaCl 0.9 wt.% before use. Human whole blood was collected in sodium citrate tubes and labeled with 5 µM DIOC6, then NPs were added to a concentration of 1 mg/mL. The blood was then perfused at venous shear stress (here, 7 µL/min) for 2 min after 0 min or 30 min incubation in blood and fluorescence images were acquired with a microscope (Axio Observer, Carl Zeiss Microscopy, Oberkochen, Germany). Fluorescence was measured across 5 cross-sections per channel and averaged over 2 min for each sample.

In flow platelet aggregates targeting assay: An *in vitro* flow adhesion assay was performed to evaluate the targeting of NPs to activated platelets. Micro-channels of Vena8 Fluoro+ chambers (width: 0.04 cm, height: 0.01 cm, and length: 2.8 cm; Cellix Ltd, Dublin, Ireland) were coated overnight with fibrillar type I collagen (50 µg/mL) overnight at 4°C and rinsed with NaCl 0.9 wt.% before use. Human whole blood, collected in the PPACK tubes and labeled with 5 µM DIOC6, was perfused at arterial shear stress (here, 60 µL/min) for 5 min to induce platelet activation and aggregation. Platelet aggregation through contact with collagen was visualized in real-time with a microscope (Axio Observer, Carl Zeiss Microscopy, Oberkochen, Germany). After rinsing with NaCl 0.9 wt.%, fluorescent Dex-NPs or Fuco-NPs (unloaded or loaded with rtPA) resuspended in 0.9 wt.% NaCl at 1 mg/mL, were injected into the channels for 5 min. Their accumulation on activated aggregates was monitored in real time. Channels were then washed for 5 min with NaCl 0.9 wt.%. Finally, quantification of bound NPs to aggregated platelets was performed with ImageJ by measuring the total fluorescence intensity and colocalization with the Pearson's coefficient (with a PSF size of 6x6 pixels) on mosaic images composed of 10 aligned microscope images (corresponding to a whole channel).

Drug loading: rtPA was loaded onto the NPs by adsorption. Typically, 50 µL of NPs (5 mg/mL) were mixed with 25 µL rtPA (1 mg/mL) and 25 µL ultrapure water then incubated for 15 min. Free unabsorbed rtPA was removed by ultracentrifugation (15 min, 15 000 g). The rtPA loaded NPs were resuspended in ultrapure water, and rtPA encapsulation was determined as described below by BCA and PefaFluor tPA assays. DNase I was loaded onto the NPs by adsorption in acidic conditions. Typically, 25 µL of NPs (10 mg/mL) were mixed with 50 µL DNase I (1 mg/mL), 5 µL of HCl (2.10^{-2} M), 10 µL $CaCl_2$ (650 µM) and 10 µL ultrapure water then incubated for 15 min. Free unabsorbed DNase I was removed by ultracentrifugation (15 min, 15 000 g). The DNase I loaded NPs were resuspended in

130 µM $CaCl_2$ and DNase I encapsulation was determined as described below by BCA and a fluorescent substrate DNAse detection kit assays.

Drug encapsulation efficiency and release rates: The amount of drug (rtPA or DNase I) loaded on the NPs was measured using the Pierce BCA protein assay kit (Life Technologies SAS, Courtaboeuf, France). Briefly, 200 µL of working reagent was added to 25 µL of each sample in 96 wells multiplate. The absorbance at 562 nm was read with a Varioskan LUX multiplate reader (Thermo Fisher Scientific, Massachusetts, United States) after 30 min incubation at 37°C. The concentration of the drug was extrapolated by a calibration curve prepared with different concentrations of rtPA or DNase I. The encapsulation efficacy (EE) was calculated as EE (%) = 100% x $[Drug]_{loaded}/[Drug]_{initial}$ and the loading capacity (LC) was calculated as LC (%) = 100% x $[Drug]_{loaded}/[NP]$. The release of each drug was investigated by diluting drug-loaded NPs (2.5 mg/mL NPs, loaded with respectively 167.5 µg/mL rtPA or 450 µg/mL DNase I) in PBS 1X in order to achieve equivalent respective drug concentrations of 1 mg/kg rtPA and 5 mg/kg DNase I in humans. This corresponds to a dilution by a factor 13X for rtPA (diluting from 167.5 µg/mL to 12.8 µg/mL rtPA) and by a factor 7X for DNase I (diluting from 450 to 64 µg/mL DNase I). During incubation at 37°C, supernatant samples are taken at regular intervals with respectively ultracentrifugation and ultrafiltration, then concentrations in supernatants is measured with respectively PefaFluor and DNase detection kits.

Fibrin Agar Plate Assay (FAPA): To assess the fibrinolytic activity of rtPA-loaded Fuco-NPs, a fibrinolysis experiment was performed. 5 mL of TBS Buffer (0.1 M Tris, 0.8 wt.% NaCl, 0.02 wt.% KCl, pH = 7.4) with 3 wt.% low melting agarose were heated above 65 °C, while 5 mL of TBS buffer with 25 mg fibrinogen and 1 U plasminogen was slowly heated to 37 °C. Once the agarose solution reached 65 °C, it was cooled to 37°C, and 2 U of thrombin were added. Next, the two solutions were slowly mixed, then poured into a 9 cm Petri dish and incubated at 37 °C for 2 h (gels can be kept a few days at 4°C). On the solidified agarose gel, round wells were formed using a 3 mm punch as sample reservoirs. 5 µL of each sample (diluted 1:10) was dropped into the wells and incubated at 37 °C in a humid environment. Pictures were taken every hour for a commercial smartphone (64 MP F1.8 OIS camera) for 8 h. The degree of fibrin lysis was quantified with ImageJ by comparing the rate of expansion for fibrinolysis rings between samples and free rtPA standards as per the method described in Wang *et al*., 2012.[39]

NET degradation assay: To assess the NETolytic activity of DNase I-loaded NPs, a semiquantitative assay was performed. Human whole blood was collected in EDTA tubes. Following the supplier's protocol for Polymorphprep, neutrophils were isolated and resuspended in 0.05 wt.% BSA in DMEM. Purity and cell count were determined with a hematology analyzer (ABX Pentra 60, Horiba, Vénissieux, France). Neutrophils were seeded at 1.0 x 10^5 cells/cm^2 on 8-wells Lab-Tek II Chamber Slide (Thermo Fischer Scientific, Massachusetts, United States) and incubated at a humidified atmosphere of 5% CO_2 for 60 min. PMA was then added to a final concentration of 50 nM, and the neutrophils were left to incubate for 4 h. Medium was then changed to incubate the formed NETs with DNase I-loaded Fuco-NPs resuspended in 0.05 wt.% BSA-DMEM to a concentration equivalent to 0.5 or 0.1 mg/mL DNase I. After a 60 min incubation, the samples were fixed with 4% (v/v) paraformaldehyde for 30 min at RT. After rinsing three times with PBS, the samples were blocked with 1% BSA in 0.1% (v/v) Tween 20 PBS (PBS-T) for 30 min at RT, then washed with PBS three times. Then, the samples were incubated with 100 nM SytoxGreen and 1 µg/mL DAPI in 1 wt.% BSA PBS-T for 10 min at RT, then washed with PBS twice before slide mounting and imaging with a microscope (Axio Observer, Carl Zeiss Microscopy, Oberkochen, Germany).

***In vitro* static thrombolysis:** For static thrombolysis assays, two types of blood clots were prepared *in vitro*: "young" and "old" clots. Human whole blood was collected in sodium citrate tubes, and 200 µL blood were added to glass tubes containing 10 µL water with 200 mM $CaCl_2$ and 2 U/mL thrombin. The tubes were closed and incubated at 37°C for 1 h for "young" clots. For "old" clots, 0.2 U/mL thrombin and 24 h incubation were used. The resulting clots were washed four times in PBS, weighted, and then washed again three times. The clots were then incubated at 37 °C with the different conditions (resuspended in PBS, with 0.25 U of plasminogen added per clot) for 1 h with slow agitation. The clots were weighted again, and the supernatants were frozen at -20 °C for 24 h. Quantification of released hemoglobin (Hb) was performed by thawing the supernatants and then mixing twenty volumes of Drabkin's reagent (200 mg/L potassium ferricyanide, 50 mg/L potassium cyanide, 140 mg/L potassium dihydrogen phosphate, 1% (v/v) Tween 20, pH = 7-7.4) with one volume supernatant. After 10 min incubation in the dark at RT, absorbance is read at 540 nm with a Varioskan LUX multiplate reader (Thermo Fisher Scientific, Massachusetts, United States). rtPA and DNase I

concentrations used were 1 and 50 µg/mL respectively. For NET content quantification, untreated “young” and “old” clots were retrieved after the first four PBS washes, and then fixed with 4% (v/v) paraformaldehyde for 24 h at 4°C. After washing three times with PBS, clots were incubated at RT for 30 min with 100 nM SytoxGreen and 1 µg/mL DAPI in PBS, then washed three times before imaging with a Leica Z16 APO macroscope (Leica, Nanterre, France) equipped with an Orca Flash 4.0 LT camera (Hamamatsu, Hamamatsu City, Japan). To assess thrombus structure, the thrombi were then fixed with 4% (v/v) paraformaldehyde for 24 h at 4 °C, and then embedded in paraffin. For each clot, two slices at different levels were stained with hematoxylin-eosin and natural saffron (HES). Digital slides from tissue slices were acquired using a Nanozoomer (Hamamatsu, Hamamatsu City, Japan) and the histological analysis was performed with QuPath 0.5.1 with pixel classification (RBCs, fibrin, immune cells) trained on two separate images.

***In vivo* FeCl3 mesenteric vein thrombosis model:** Animal studies were performed on 6–8 week old C57BL6J mice (Janvier Labs, Le Genest-Saint-Isle, France), with equipartition of males (24.9 ± 2.3 g weight) and females (19.9 ± 2.4 g weight) in each group. All experiments were adapted according to French (Decree 87/848) and European (2010/63/EU) ethical guidelines. The local ethic committee (C2EA-121 Paris Nord, France) and the French Ministère de l’Enseignement Supérieur et de la Recherche approved the fulfilling of the experiments with the reference number APAFIS #45198-2023092014273800. After an acclimatation period of one week in an enriched environment, mice received analgesia (subcutaneous injection of buprenorphine 0.05 mg/kg), and then anesthetized for the whole procedure (4% isoflurane inhalation for initiation and then continuous 2% isoflurane inhalation). A midline abdominal incision was performed to expose the mesentery, which was gently laid out over a transparent Petri dish and placed under an intravital macroscope: Leica Z16 APO macroscope (Leica, Nanterre, France) equipped with an Orca Flash 4.0 LT camera (Hamamatsu, Hamamatsu City, Japan). A retro-orbital injection of 30 µL of DIOC6 50 µM was performed to label leukocytes and platelets. A 1 mm large Whatmann chromatography paper band, previously soaked in 10 wt.% $FeCl_3$ was deposed on a mesentery vein for one minute before removal. Thrombus formation was observed in real time for 10 to 20 min by fluorescence macroscopy. Once the thrombus was formed, images were acquired at 20 s intervals for 30 min. Between the second and third frames, samples were administered

with a retro-orbital injection (150 µL injections, in a saline suspension). When NPs were used, they were fluorescently labeled with TRITC, and the maximum final concentration of Fuco-NPs in the mice blood was 962 ± 26 µg/mL (obtained for Fuco-NP-rtPA 5 mg/kg and empty Fuco-NPs). At the end of image acquisition, the animals were sacrificed. Image analysis of thrombi with ImageJ included a SIFT-based alignment with a rigid transformation. The thrombus area was measured over time in the DIOC6 channel to create thrombi binary masks by thresholding, and the rate of thrombus degradation was analyzed after the thrombus reached its maximum size in the first 20 frames (7 min). For targeting measurements, the mean fluorescence intensity (MFI) was measured in the thrombus for both DIOC6 and TRITC over time, and in particular after 30 min as a ratio of MFI_{TRITC}/MFI_{DIOC6}.

Inflammatory response in mice: Animal studies were performed on 6–8 week old C57BL6J mice (Janvier Labs, Le Genest Saint Isle, France), with equipartition of males and females in each group. All experiments were adapted according to French (Decree 87/848) and European (2010/63/EU) ethical guidelines. The local ethic committee (C2EA-121 Paris Nord, France) and the French Ministère de l'Enseignement Supérieur et de la Recherche approved the fulfilling of the experiments with the reference number APAFIS #49260-2024032517159016. After an acclimatation period of one week in an enriched environment, mice were anesthetized (4% isoflurane inhalation) then Fuco-NPs at the equivalent concentration of 1 mg/kg rtPA delivery in human were administered retro-orbital injection (150 µL injections, in saline suspension). A topical ophthalmic anesthetic (tetracaine 1%) was applied before the animal woke up. The animals were then kept for 1, 3 or 24 h with a general inspection at 1 h to check end points. The animals were then sacrificed, and the liver, spleen, kidney, lung and blood samples were harvested. The resulting plasma was used to measure the level of several inflammatory cytokines by a MultiPlex assay (Bio-Plex Pro Mouse Cytokine 8-plex Assay #M60000007A) with a Bio-Plex 200 system (Bio-Rad, Marnes-la-Coquette, France).

Biodistribution in mice: For a limited number of animals (n=4) and for the saline and Fuco-NP conditions, organs (liver, spleen, kidney, and lung) were harvested after the *in vivo* thrombosis model described above. They were fixed with 4% (v/v) paraformaldehyde for 24 h at 4°C, and then transferred in 70% EtOH for storage. The organs were later embedded in paraffin. For each organ, representative slices were stained with

hematoxylin, eosin, and natural saffron (HES) and Alcian Blue (AB). Furthermore, for one animal for each condition, immunohistochemistry (IHC) was performed. Briefly, after deparaffinization, rehydration, and antigen retrieval (citric acid buffer, pH = 6), slides were incubated with a primary anti-CD68 antibody (dilution 1:100) and then the supplier's protocol was followed for the IHC detection kit with horse radish peroxidase (HRP), with an acid Mayer's hemalum counterstaining. Digital slides from tissue slices were acquired using a Nanozoomer (Hamamatsu, Hamamatsu City, Japan).

Image analysis and statistical analysis: Images were analyzed with ImageJ (Fiji), and the macros that were used are made available in Supporting Information. When images are shown, the same contrast values are applied to each channel displayed. Quantitative data were analyzed with the statistical analysis software GraphPad PRISM 9.5.0., with a significance level α taken at 0.05. All presented data consisted of n = 3 or more replicates per condition (when not shown on the graphs, replicate number is indicated in the legend). Whenever applicable, the presented replicates consist of biological replicates, or, when appropriate, different NP batches. Unless explicitly mentioned, results are presented as mean ± standard deviation. Depending on the design of the experiments, data significance was evaluated with unpaired t-test (two groups, assumed equal variance), unpaired t-test with Welch's correction (two groups, variance not equal), paired t-test (two groups of paired values, with assumed equal variance), one-way ANOVA (one factor explored, with more than two groups, variances assumed equal) with Tukey's multiple comparison test, one-way Welch's ANOVA (one factor explored, with more than two groups, variances not equal) with Dunnett's T3 multiple comparison test, repeated measures one-way ANOVA (one factor explored, with more than two groups of repeated measures compared to the initial group, variances assumed equal) with Dunnett's multiple comparison test, and two-way ANOVA (two factors explored) with Tukey's multiple comparison test. Unless explicitly specified in the legend, unpaired t-tests and ANOVA with Tukey's test are performed. Every p-value below α threshold was represented as follows: * $p < 0.05$; ** $p < 0.01$; *** $p < 0.001$, **** $p < 0.0001$ (ns was indicated for "not significant" if no significant differences are present in the data presented).

Acknowledgments

The authors thank INSERM, Université Sorbonne Paris Nord, Université Paris Cité with the STRATEX “Reprobulles” RM27J22IDX87 and the ANR “FightClot” ANR-20-CE18-0005-01 for the financial support. They also express their gratitude to Algues & Mer for the supply of fucoidan. The authors would like to acknowledge Thomas BONNARD, Alina ZENYCH and Laura FORERO-RAMIREZ for the initial design of submicronic particles, Stéphane LOYAU for his help and expertise on experiments involving human blood, Deborah FRANCOIS for her help with the animal experimentation, Yoann LALATONNE for his help with the TXRF data acquisition, Yang ZHANG for procuring the HUVECs for cytotoxicity assays. We acknowledge the ImagoSeine core facility of the Institut Jacques Monod, member of the France BioImaging infrastructure (ANR-10-INBS-04) and GIS-IBiSA, for the TEM imaging. We acknowledge Olivier THIBAUDEAU from the Morphology Platform at INSERM UMR 1152-Bichat Hospital for his help with immunohistochemistry. The illustrations were designed with BioRender online software (biorender.com). The graphical abstract was designed with BioRender and Blender 4.2, with an initial blood vessel design by Ryo Mizuta Graphics.

Supporting Information

The Supporting Information is available free of charge at https://pubs.acs.org/doi/10.1021/acsnano.4c17049).

- Supplementary Figures: Parameters and values used for the HLD equation with the synthesis conditions; TEM images; zeta potential of Dex−NPs and Fuco−NPs; FTIR spectra; freeze−drying of Fuco−NPs; in−flow behavior comparison of Fuco−NPs; hemolysis assay; degradability of Fuco−NPs by dextranase; quantification of the active rtPA−loaded in NPs measured by amidolytic PefaFluor assay; DNase I encapsulation in Fuco−NPs; stability after freeze−drying and resuspension of drug−loaded Fuco−NPs; encapsulation of both rtPA and DNase I in Fuco−NPs; targeting with NPs; static thrombolysis; histological analysis; biodistribution of Fuco−NPs in mice after thrombosis experiment; and inflammatory profile of healthy Fuco−NPs treated mice (PDF)

- ImageJ Macros: ImageJ Macros used for image analysis (TXT)
- Supplementary Movies 1-5: representative flow targeting assays in microfluidic channels for Fig.4.a-b and Sup.Fig.15.a-b (AVI)
- Supplementary Movies 6-15: *in vivo* thrombolysis representative experiments for Sup.Fig.15.c and Fig.5 (AVI)

Author Contributions

Thibault DE LA TAILLE: Conceptualization, Methodology, Investigation, Experimental work, Data Curation, Writing - Original Draft, Visualization; Pierre SARFATI: Methodology, Investigation; Rachida AID: Methodology, Investigation; Louise FOURNIER: Methodology; Graciela PAVON-DJAVID: Methodology, Investigation; Frédéric CHAUBET: Conceptualization, Resources, Writing - Review and Editing, Supervision, Project administration, Funding acquisition; Cédric CHAUVIERRE: Conceptualization, Resources, Writing - Review and Editing, Supervision, Project administration, Funding acquisition. All the authors approved the final revised version of the manuscript.

Abbreviations

CVD, cardiovascular disease; IHD, ischemic heart disease; AIS, acute ischemic stroke; DALYs, disability-adjusted life years; MI, myocardial infarction; VWF, Von Willebrand factor; NET, neutrophil extracellular trap; rtPA, recombinant tissue plasminogen activator; EVT, endovascular therapy; NP, nanoparticle; HLD, hydrophilic lipophilic difference; EACN, effective alkane carbon number; Cc, characteristic curvature; PDI, polydispersity; LC, loading capacity; EE, encapsulation efficacy; Hb, hemoglobin; IHC, immunohistochemistry; HES, hematoxylin-eosin and natural saffron; AB, Alcian Blue; MPS, mononuclear phagocyte system; TEM, transmission electron microscopy.

References

(1) Ferrari, A. J.; Santomauro, D. F.; Aali, A.; Abate, Y. H.; Abbafati, C.; Abbastabar, H.; ElHafeez, S. A.; Abdelmasseh, M.; Abd-Elsalam, S.; Abdollahi, A.; Abdullahi, A.;

Abegaz, K. H.; Zuñiga, R. A. A.; Aboagye, R. G.; Abolhassani, H.; Abreu, L. G.; Abualruz, H.; Abu-Gharbieh, E.; Abu-Rmeileh, N. M.; Ackerman, I. N.; et al. Global Incidence, Prevalence, Years Lived with Disability (YLDs), Disability-Adjusted Life-Years (DALYs), and Healthy Life Expectancy (HALE) for 371 Diseases and Injuries in 204 Countries and Territories and 811 Subnational Locations, 1990–2021: A Systematic Analysis for the Global Burden of Disease Study 2021. *The Lancet* **2024**, *403* (10440), 2133–2161.

(2) Alkarithi, G.; Duval, C.; Shi, Y.; Macrae, F. L.; Ariëns, R. A. S. Thrombus Structural Composition in Cardiovascular Disease. *Arterioscler. Thromb. Vasc. Biol.* **2021**, *41* (9), 2370–2383.

(3) Di Meglio, L.; Desilles, J.-P.; Ollivier, V.; Nomenjanahary, M. S.; Di Meglio, S.; Deschildre, C.; Loyau, S.; Olivot, J.-M.; Blanc, R.; Piotin, M.; Bouton, M.-C.; Michel, J.-B.; Jandrot-Perrus, M.; Ho-Tin-Noé, B.; Mazighi, M. Acute Ischemic Stroke Thrombi Have an Outer Shell That Impairs Fibrinolysis. *Neurology* **2019**, *93* (18), e1686–e1698.

(4) National Institute of Neurological Disorders and Stroke rt-PA Stroke Study Group. Tissue Plasminogen Activator for Acute Ischemic Stroke. *N. Engl. J. Med.* **1995**, *333* (24), 1581–1587.

(5) Bhatia, R.; Hill, M. D.; Shobha, N.; Menon, B.; Bal, S.; Kochar, P.; Watson, T.; Goyal, M.; Demchuk, A. M. Low Rates of Acute Recanalization With Intravenous Recombinant Tissue Plasminogen Activator in Ischemic Stroke. *Stroke* **2010**, *41* (10), 2254–2258.

(6) de Havenon, A.; Sheth, K.; Johnston, K. C.; Delic, A.; Stulberg, E.; Majersik, J.; Anadani, M.; Yaghi, S.; Tirschwell, D.; Ney, J. Acute Ischemic Stroke Interventions in the United States and Racial, Socioeconomic, and Geographic Disparities. *Neurology* **2021**, *97* (23), e2292–e2303.

(7) Lapergue, B.; Blanc, R.; Costalat, V.; Desal, H.; Saleme, S.; Spelle, L.; Marnat, G.; Shotar, E.; Eugene, F.; Mazighi, M.; Houdart, E.; Consoli, A.; Rodesch, G.; Bourcier, R.; Bracard, S.; Duhamel, A.; Ben Maacha, M.; Lopez, D.; Renaud, N.; Labreuche, J.; et al. Effect of Thrombectomy With Combined Contact Aspiration and Stent Retriever vs Stent Retriever Alone on Revascularization in Patients With Acute

Ischemic Stroke and Large Vessel Occlusion: The ASTER2 Randomized Clinical Trial. *JAMA* **2021**, *326* (12), 1158–1169.

(8) Rai, A. T.; Link, P. S.; Domico, J. R. Updated Estimates of Large and Medium Vessel Strokes, Mechanical Thrombectomy Trends, and Future Projections Indicate a Relative Flattening of the Growth Curve but Highlight Opportunities for Expanding Endovascular Stroke Care. *J. NeuroInterventional Surg.* **2023**, *15* (e3), e349–e355.

(9) Ducroux, C.; Di Meglio, L.; Loyau, S.; Delbosc, S.; Boisseau, W.; Deschildre, C.; Ben Maacha, M.; Blanc, R.; Redjem, H.; Ciccio, G.; Smajda, S.; Fahed, R.; Michel, J.-B.; Piotin, M.; Salomon, L.; Mazighi, M.; Ho-Tin-Noe, B.; Desilles, J.-P. Thrombus Neutrophil Extracellular Traps Content Impair tPA-Induced Thrombolysis in Acute Ischemic Stroke. *Stroke* **2018**, *49* (3), 754–757.

(10) Peña-Martínez, C.; Durán-Laforet, V.; García-Culebras, A.; Ostos, F.; Hernández-Jiménez, M.; Bravo-Ferrer, I.; Pérez-Ruiz, A.; Ballenilla, F.; Díaz-Guzmán, J.; Pradillo, J. M.; Lizasoain, I.; Moro, M. A. Pharmacological Modulation of Neutrophil Extracellular Traps Reverses Thrombotic Stroke tPA (Tissue-Type Plasminogen Activator) Resistance. *Stroke* **2019**, *50* (11), 3228–3237.

(11) Novotny, J.; Oberdieck, P.; Titova, A.; Pelisek, J.; Chandraratne, S.; Nicol, P.; Hapfelmeier, A.; Joner, M.; Maegdefessel, L.; Poppert, H.; Pircher, J.; Massberg, S.; Friedrich, B.; Zimmer, C.; Schulz, C.; Boeckh-Behrens, T. Thrombus NET Content Is Associated with Clinical Outcome in Stroke and Myocardial Infarction. *Neurology* **2020**, *94* (22), e2346–e2360.

(12) Colasuonno, M.; Palange, A. L.; Aid, R.; Ferreira, M.; Mollica, H.; Palomba, R.; Emdin, M.; Del Sette, M.; Chauvierre, C.; Letourneur, D.; Decuzzi, P. Erythrocyte-Inspired Discoidal Polymeric Nanoconstructs Carrying Tissue Plasminogen Activator for the Enhanced Lysis of Blood Clots. *ACS Nano* **2018**, *12* (12), 12224–12237.

(13) Sarfati, P.; de La Taille, T.; Portioli, C.; Spanò, R.; Lalatonne, Y.; Decuzzi, P.; Chauvierre, C. REVIEW: “ISCHEMIC STROKE: From Fibrinolysis to Functional Recovery” Nanomedicine: Emerging Approaches to Treat Ischemic Stroke. *Neuroscience* **2024**, *550*, 102–113.

(14) Lee, T.-R.; Choi, M.; Kopacz, A. M.; Yun, S.-H.; Liu, W. K.; Decuzzi, P. On the Near-Wall Accumulation of Injectable Particles in the Microcirculation: Smaller Is Not Better. *Sci. Rep.* **2013**, *3* (1), 2079.

(15) Müller, K.; Fedosov, D. A.; Gompper, G. Margination of Micro- and Nano-Particles in Blood Flow and Its Effect on Drug Delivery. *Sci. Rep.* **2014**, *4* (1), 4871.

(16) D'Apolito, R.; Tomaiuolo, G.; Taraballi, F.; Minardi, S.; Kirui, D.; Liu, X.; Cevenini, A.; Palomba, R.; Ferrari, M.; Salvatore, F.; Tasciotti, E.; Guido, S. Red Blood Cells Affect the Margination of Microparticles in Synthetic Microcapillaries and Intravital Microcirculation as a Function of Their Size and Shape. *J. Control. Release Off. J. Control. Release Soc.* **2015**, *217*, 263–272.

(17) Duan, X.; Li, Y. Physicochemical Characteristics of Nanoparticles Affect Circulation, Biodistribution, Cellular Internalization, and Trafficking. *Small* **2013**, *9* (9–10), 1521–1532.

(18) Inggrid Setyawati, M.; Yong Tay, C.; Docter, D.; H. Stauber, R.; Tai Leong, D. Understanding and Exploiting Nanoparticles' Intimacy with the Blood Vessel and Blood. *Chem. Soc. Rev.* **2015**, *44* (22), 8174–8199.

(19) Pawlowski, C. L.; Li, W.; Sun, M.; Ravichandran, K.; Hickman, D.; Kos, C.; Kaur, G.; Sen Gupta, A. Platelet Microparticle-Inspired Clot-Responsive Nanomedicine for Targeted Fibrinolysis. *Biomaterials* **2017**, *128*, 94–108.

(20) Zhang, N.; Ru, B.; Hu, J.; Xu, L.; Wan, Q.; Liu, W.; Cai, W.; Zhu, T.; Ji, Z.; Guo, R.; Zhang, L.; Li, S.; Tong, X. Recent Advances of CREKA Peptide-Based Nanoplatforms in Biomedical Applications. *J. Nanobiotechnology* **2023**, *21*, 77.

(21) Xu, J.; Zhang, Y.; Xu, J.; Liu, G.; Di, C.; Zhao, X.; Li, X.; Li, Y.; Pang, N.; Yang, C.; Li, Y.; Li, B.; Lu, Z.; Wang, M.; Dai, K.; Yan, R.; Li, S.; Nie, G. Engineered Nanoplatelets for Targeted Delivery of Plasminogen Activators to Reverse Thrombus in Multiple Mouse Thrombosis Models. *Adv. Mater.* **2020**, *32* (4), 1905145.

(22) Xu, J.; Wang, X.; Yin, H.; Cao, X.; Hu, Q.; Lv, W.; Xu, Q.; Gu, Z.; Xin, H. Sequentially Site-Specific Delivery of Thrombolytics and Neuroprotectant for Enhanced Treatment of Ischemic Stroke. *ACS Nano* **2019**, *13* (8), 8577–8588.

(23) Niu, Y.; Tan, H.; Li, X.; Zhao, L.; Xie, Z.; Zhang, Y.; Zhou, S.; Qu, X. Protein–Carbon Dot Nanohybrid-Based Early Blood–Brain Barrier Damage Theranostics. *ACS Appl. Mater. Interfaces* **2020**, *12* (3), 3445–3452.

(24) Guan, L.; Wang, C.; Yan, X.; Liu, L.; Li, Y.; Mu, Y. Author Correction: A Thrombolytic Therapy Using Diagnostic Ultrasound Combined with RGDS-Targeted Microbubbles and Urokinase in a Rabbit Model. *Sci. Rep.* **2020**, *10* (1), 15767.

(25) Akbarzadeh, A.; Rezaei-Sadabady, R.; Davaran, S.; Joo, S. W.; Zarghami, N.; Hanifehpour, Y.; Samiei, M.; Kouhi, M.; Nejati-Koshki, K. Liposome: Classification, Preparation, and Applications. *Nanoscale Res. Lett.* **2013**, *8* (1), 102.

(26) Perkins, L. A.; Anderson, C. J.; Novelli, E. M. Targeting P-Selectin Adhesion Molecule in Molecular Imaging: P-Selectin Expression as a Valuable Imaging Biomarker of Inflammation in Cardiovascular Disease. *J. Nucl. Med.* **2019**, *60* (12), 1691–1697.

(27) Chauvierre, C.; Aid-Launais, R.; Aerts, J.; Chaubet, F.; Maire, M.; Chollet, L.; Rolland, L.; Bonafé, R.; Rossi, S.; Bussi, S.; Cabella, C.; Dézsi, L.; Fülöp, T.; Szebeni, J.; Chahid, Y.; Zheng, K. H.; Stroes, E. S. G.; Le Guludec, D.; Rouzet, F.; Letourneur, D. Pharmaceutical Development and Safety Evaluation of a GMP-Grade Fucoidan for Molecular Diagnosis of Cardiovascular Diseases. *Mar. Drugs* **2019**, *17* (12), 699.

(28) Zheng, K. H.; Kaiser, Y.; Poel, E.; Verberne, H.; Aerts, J.; Rouzet, F.; Stroes, E.; Letourneur, D.; Chauvierre, C. 99Mtc-Fucoidan As Diagnostic Agent For P-Selectin Imaging: First-In-Human Evaluation (Phase I). *Atherosclerosis* **2019**, *287*, e143.

(29) Bonnard, T.; Yang, G.; Petiet, A.; Ollivier, V.; Haddad, O.; Arnaud, D.; Louedec, L.; Bachelet-Violette, L.; Derkaoui, S. M.; Letourneur, D.; Chauvierre, C.; Visage, C. L. Abdominal Aortic Aneurysms Targeted by Functionalized Polysaccharide Microparticles: A New Tool for SPECT Imaging. *Theranostics* **2014**, *4* (6), 592–603.

(30) Zenych, A.; Jacqmarcq, C.; Aid, R.; Fournier, L.; Forero Ramirez, L. M.; Chaubet, F.; Bonnard, T.; Vivien, D.; Letourneur, D.; Chauvierre, C. Fucoidan-Functionalized Polysaccharide Submicroparticles Loaded with Alteplase for Efficient Targeted Thrombolytic Therapy. *Biomaterials* **2021**, *277*, 121102.

(31) Forero Ramirez, L. M.; Gobin, E.; Aid-Launais, R.; Journe, C.; Moraes, F.; Picton, L.; Le Cerf, D.; Letourneur, D.; Chauvierre, C.; Chaubet, F. Gd(DOTA)-Grafted Submicronic Polysaccharide-Based Particles Functionalized with Fucoidan as Potential MR Contrast Agent Able to Target Human Activated Platelets. *Carbohydr. Polym.* **2020**, *245*, 116457.

(32) Abbott, S. J. *Surfactant Science: Principles & Practice*; DEStech Publications, Incorporated, 2017.

(33) Lovell, P. A.; Schork, F. J. Fundamentals of Emulsion Polymerization. *Biomacromolecules* **2020**, *21* (11), 4396–4441.

(34) Hong, C.; Alser, O.; Gebran, A.; He, Y.; Joo, W.; Kokoroskos, N.; Velmahos, G.; Olsen, B. D.; Hammond, P. T. Modulating Nanoparticle Size to Understand Factors Affecting Hemostatic Efficacy and Maximize Survival in a Lethal Inferior Vena Cava Injury Model. *ACS Nano* **2022**, *16* (2), 2494–2510.

(35) Gruber, S.; Nickel, A. Toxic or Not Toxic? The Specifications of the Standard ISO 10993-5 Are Not Explicit Enough to Yield Comparable Results in the Cytotoxicity Assessment of an Identical Medical Device. *Front. Med. Technol.* **2023**, *5*, 1195529.

(36) Guo, S.; Shi, Y.; Liang, Y.; Liu, L.; Sun, K.; Li, Y. Relationship and Improvement Strategies between Drug Nanocarrier Characteristics and Hemocompatibility: What Can We Learn from the Literature. *Asian J. Pharm. Sci.* **2021**, *16* (5), 551–576.

(37) Fournier, L.; Abioui-Mourgues, M.; Chabouh, G.; Aid, R.; Taille, T. D. L.; Couture, O.; Vivien, D.; Orset, C.; Chauvierre, C. rtPA-Loaded Fucoidan Polymer Microbubbles for the Targeted Treatment of Stroke. *Biomaterials* **2023**, *303*, 122385.

(38) Orset, C.; Macrez, R.; Young, A. R.; Panthou, D.; Angles-Cano, E.; Maubert, E.; Agin, V.; Vivien, D. Mouse Model of In Situ Thromboembolic Stroke and Reperfusion. *Stroke* **2007**, *38* (10), 2771–2778.

(39) Wang, M.; Yang, W.; Wu, Q.; Gu, H. Modeling of the Fibrin Agarose Plate Assay and Its Application for Thrombolytic Analysis. *Chin. Sci. Bull.* **2012**, *57*.

(40) Jiménez-Alcázar, M.; Napirei, M.; Panda, R.; Köhler, E. C.; Kremer Hovinga, J. A.; Mannherz, H. G.; Peine, S.; Renné, T.; Lämmle, B.; Fuchs, T. A. Impaired DNase1-mediated Degradation of Neutrophil Extracellular Traps Is Associated with Acute Thrombotic Microangiopathies. *J. Thromb. Haemost.* **2015**, *13* (5), 732–742.

(41) Fitzgerald, S. T.; Liu, Y.; Dai, D.; Mereuta, O. M.; Abbasi, M.; Larco, J. L. A.; Douglas, A. S.; Kallmes, D. F.; Savastano, L.; Doyle, K. M.; Brinjikji, W. Novel Human Acute Ischemic Stroke Blood Clot Analogs for In Vitro Thrombectomy Testing. *AJNR Am. J. Neuroradiol.* **2021**, *42* (7), 1250–1257.

(42) Powers, W. J.; Rabinstein, A. A.; Ackerson, T.; Adeoye, O. M.; Bambakidis, N. C.; Becker, K.; Biller, J.; Brown, M.; Demaerschalk, B. M.; Hoh, B.; Jauch, E. C.; Kidwell, C. S.; Leslie-Mazwi, T. M.; Ovbiagele, B.; Scott, P. A.; Sheth, K. N.; Southerland, A. M.; Summers, D. V.; Tirschwell, D. L. Guidelines for the Early Management of

Patients With Acute Ischemic Stroke: 2019 Update to the 2018 Guidelines for the Early Management of Acute Ischemic Stroke: A Guideline for Healthcare Professionals From the American Heart Association/American Stroke Association. *Stroke* **2019**, *50* (12), e344–e418.

(43) Liu, L.; Chen, W.; Zhou, H.; Duan, W.; Li, S.; Huo, X.; Xu, W.; Huang, L.; Zheng, H.; Liu, J.; Liu, H.; Wei, Y.; Xu, J.; Wang, Y. Chinese Stroke Association Guidelines for Clinical Management of Cerebrovascular Disorders: Executive Summary and 2019 Update of Clinical Management of Ischaemic Cerebrovascular Diseases. *Stroke Vasc. Neurol.* **2020**, *5* (2), 159–176.

(44) Gurewich, V. Therapeutic Fibrinolysis: How Efficacy and Safety Can Be Improved. *J. Am. Coll. Cardiol.* **2016**, *68* (19), 2099–2106.

(45) Bannish, B. E.; Chernysh, I. N.; Keener, J. P.; Fogelson, A. L.; Weisel, J. W. Molecular and Physical Mechanisms of Fibrinolysis and Thrombolysis from Mathematical Modeling and Experiments. *Sci. Rep.* **2017**, *7* (1), 6914.

(46) Kraal, G.; Mebius, R. New Insights into the Cell Biology of the Marginal Zone of the Spleen. *Int. Rev. Cytol.* **2006**, *250*, 175–215.

(47) Gustafson, H. H.; Holt-Casper, D.; Grainger, D. W.; Ghandehari, H. Nanoparticle Uptake: The Phagocyte Problem. *Nano Today* **2015**, *10* (4), 487–510.

(48) Khalikova, E.; Susi, P.; Korpela, T. Microbial Dextran-Hydrolyzing Enzymes: Fundamentals and Applications. *Microbiol. Mol. Biol. Rev.* **2005**, *69* (2), 306–325.

(49) Maia, J.; Evangelista, M.; Gil, H.; Ferreira, L. Dextran-Based Materials for Biomedical Applications. In *Carbohydrates Applications in Medicine*; M.H. Gil, 2014; pp 31–53.

(50) Wang, R.; Dijkstra, P. J.; Karperien, M. Dextran. In *Biomaterials from Nature for Advanced Devices and Therapies*; John Wiley & Sons, Ltd, 2016; pp 307–319.

(51) Lee, J. M.; Shin, Z.-U.; Mavlonov, G.; Abdurakhmonov, I.; Yi, T. Solid-Phase Colorimetric Method for the Quantification of Fucoidan. *Appl. Biochem. Biotechnol.* **2012**, *168*.